Chapter 9

Boiling Heat Transfer on External Surfaces

(Revised in 2006)

SUMMARY: Boiling on the outside of tubes is surveyed in this chapter. First, nucleate pool boiling is described, which is a two-phase process analogous to single-phase natural convection since the only movement of the pool is due to the boiling process itself. Then, convective boiling on the outside of horizontal tube bundles is discussed. Topics covered include: the pool boiling curve, heat transfer mechanisms for plain and enhanced tubes, nucleate pool boiling correlations for plain tubes, critical heat flux of nucleate boiling, boiling of mixtures, boiling on enhanced tubes, and bundle boiling on plain, low fin and Turbo-B geometry tubes.

9.1 Introduction

The basics of boiling on plain tubes, enhanced tubes and tube bundles are addressed here. For other comprehensive reviews and presentations on this subject, refer to Thome (1990) for enhanced boiling and to Collier and Thome (1994) or van Stralen and Cole (1979) for the fundamentals of boiling. Another presentation on boiling heat transfer is a survey presented by Thome (1998) on research in this area in the 1990's.

9.2 Enhanced Boiling Surfaces

Numerous enhanced boiling surfaces have been proposed and patented over the years. Figure 9.1 depicts a diagram showing a variety of geometries, most which have never made it to market. The first type of enhanced boiling tube to become successful was the low finned tube. Figure 9.2 depicts a photograph of a Turbo-Chil low finned tube made by Wolverine Tube Inc.

By mechanically deforming low finned tubes, it is possible for create a high density of re-entrant channels and pores on a tube's surface, which increases heat transfer performance significantly. Figure 9.3 shows several diagrams of the Turbo-B tube made by Wolverine Tube Inc. that is widely used in refrigerant flooded evaporators, showing its external enhanced boiling geometry and its internal helical fins for augmenting heat transfer to chilled water. Figure 9.4 shows photographs of some of the various versions of the Turbo-B tubes produced by Wolverine Tube Inc.

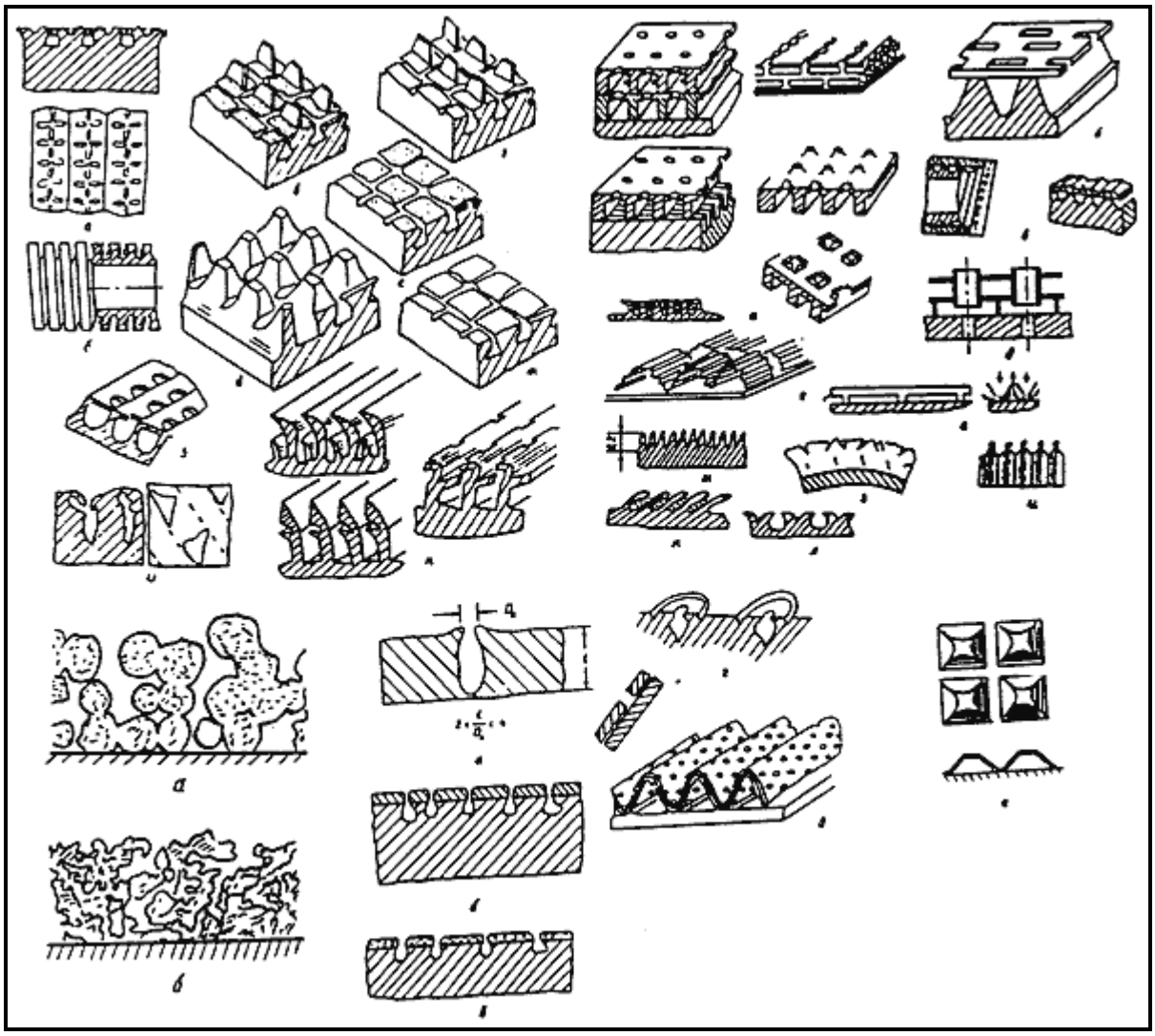

Figure 9.1. Selection of enhanced boiling surfaces.

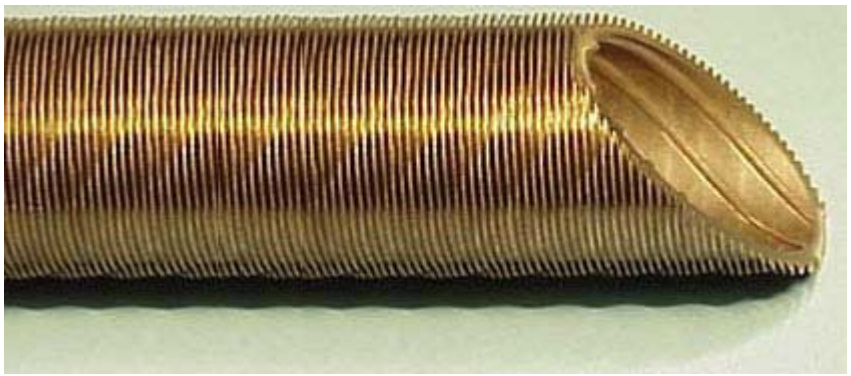

Figure 9.2. Photograph of Turbo-Chil low finned tube.

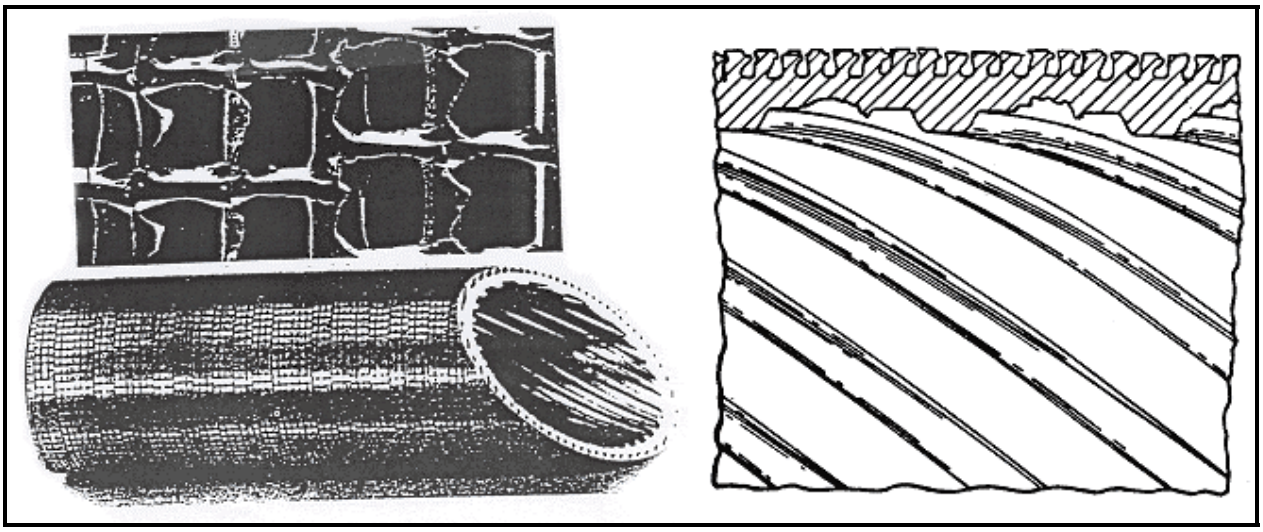

Figure 9.3. Turbo-B enhancement geometry.

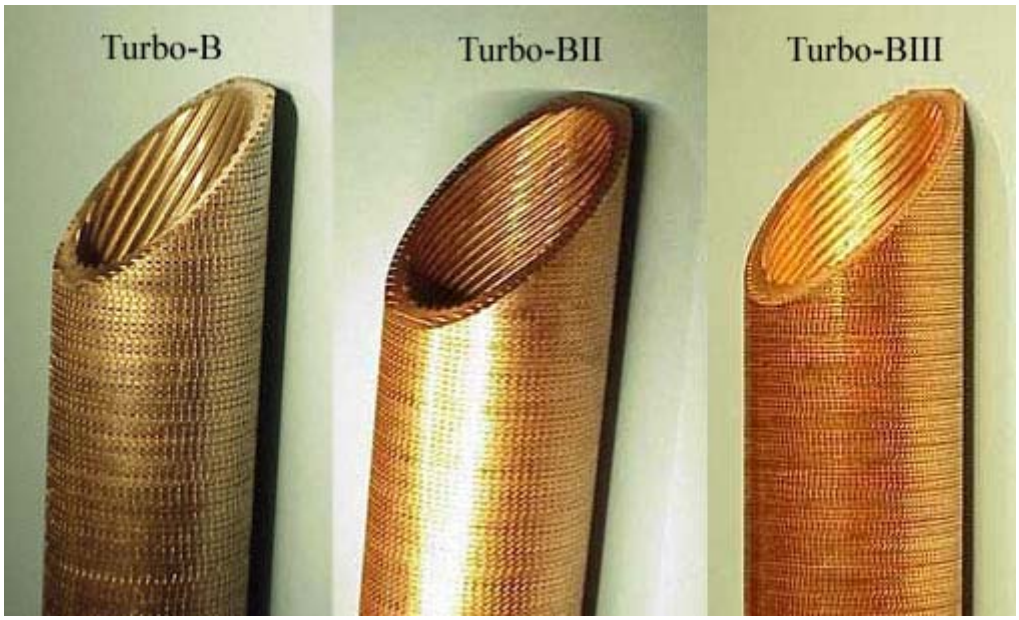

Figure 9.4. Photographs of Turbo-B, Turbo-BII and Turbo-BIII tubes.

9.3 Boiling on Plain Tubes

The most important features of pool boiling heat transfer are its characteristic pool boiling curve, the heat transfer mechanisms responsible for removing heat from the heated boiling surface, nucleate pool boiling correlations for predicting heat transfer coefficients and the maximum feasible nucleate pool boiling heat flux. These topics are discussed below.

9.3.1 Pool Boiling Heat Transfer

Consider an electrically heated wire (or tube) placed in a large pool of quiescent liquid at or near its saturation temperature. Applying Joule resistance heating and using the wire (or tube) as a resistance thermometer, its surface temperature can be measured as a function of heat flux and plotted as heat flux versus surface temperature as shown in Figure 9.5. This diagram was first presented by Nukiyama (1934) and is often referred to as Nukiyama's curve. It is more common nowadays to plot the wall heat flux q versus the temperature difference ΔT between the wall temperature T_{wall} and the saturation temperature T_{sat} on logarithmic scales, or to plot the pool boiling heat transfer coefficient α_{nb} versus the heat flux. In the curve depicted, four distinct trends of heat transfer regimes can be distinguished:

- Natural convection ($T_{wall} < T_{IB}$)
- Nucleate boiling ($T_{IB} < T_{wall} < T_{DNB}$)
- Transition boiling ($T_{DNB} < T_{wall} < T_{MFB}$)
- Film boiling ($T_{MFB} < T_{wall}$)

that are delineated by the three transition points:

- IB: the point of Incipience of Boiling (IB)
- DNB: the point of Departure from Nucleate Boiling (DNB)
- MFB: the Minimum Film Boiling point.

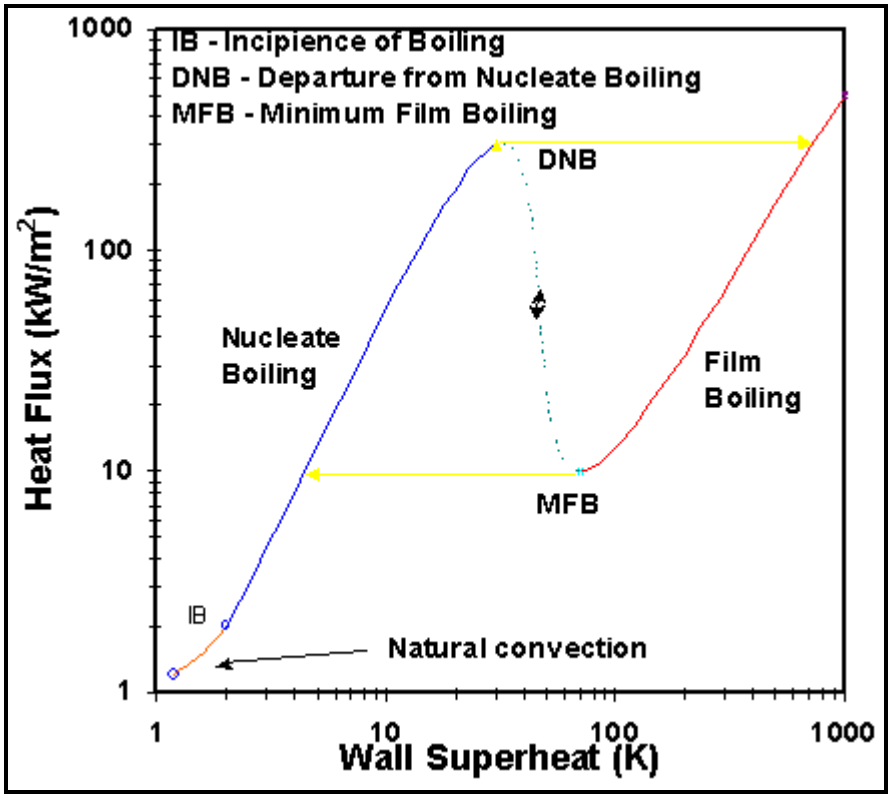

Figure 9.5. Pool boiling curve.

For increasing heat flux, first the natural convection regime is encountered the surface temperature reaches that necessary for boiling nucleation to occur at point IB. Then, the process passes up the *nucleate boiling curve* until arriving at the surface temperature at which departure from nucleate boiling (DNB) occurs, often also referred to as the critical heat flux. At this point, the process jumps to a much higher surface temperature on the *film boiling curve*. Reducing the heat flux, the process follows the film boiling curve until arriving at the surface temperature at which the film boiling process becomes unstable (MFB), a point also sometimes referred to as the Liedenfrost point. At this point, the process jumps to a lower surface temperature and rejoins the nucleate boiling curve. For experiments with a temperature controlled surface temperature rather than for a heat flux controlled process as described above, the process will pass through the *transition boiling curve* between the points DNB and MFB.

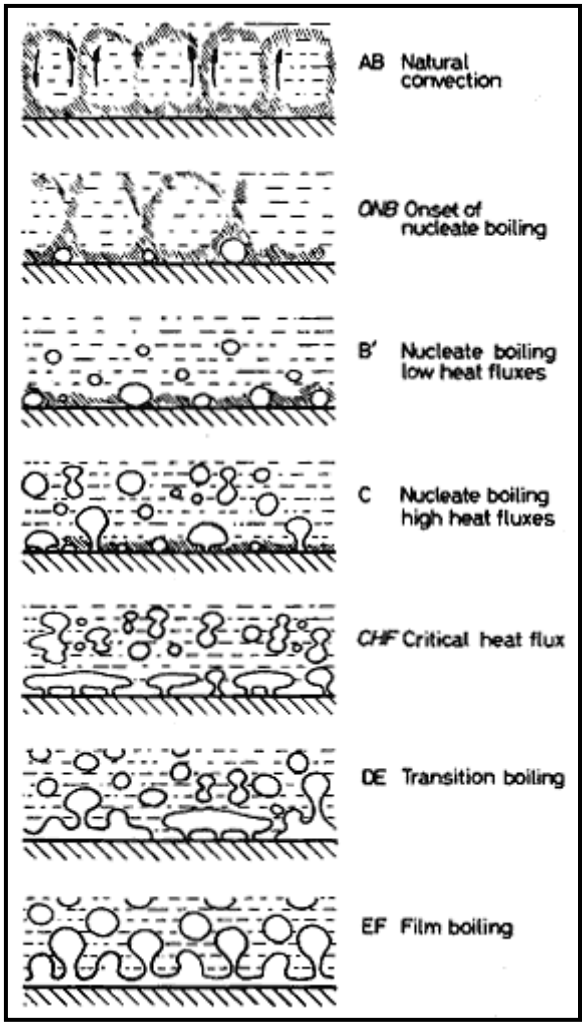

Figure 9.6. Pool boiling processes.

A schematic representation of these regimes taken from Collier and Thome (1994) is shown in Figure 9.6. The natural convection part of the curve can be predicted using well-established correlations for single-phase natural convection. In this regime the wall temperature continues to rise as the heat flux is increased until the first bubbles appear, indicating boiling nucleation on the surface (point IB). These bubbles grow from vapor trapped in small cavities in the surface and are the so-called nucleation sites. As the heat flux is increased, more and more nucleation sites become activated. On the nucleate boiling curve, large increases in heat flux are achieved for relatively modest increases in ΔT (defined as $T_{wall} - T_{sat}$) until the DNB condition is reached. At DNB, jets of rising vapor are formed that prevents liquid from reaching the heated surface, such that it becomes blanketed by vapor, which greatly degrades heat transfer. On the film boiling region of the curve, the wall is completely covered with a thin film of vapor. Heat is transferred by heat conduction and radiation from the wall through the vapor film. The vapor film is stable in that liquid does not normally wet the heater surface, although some transient wetting may occur, and at the free interface between the film and the liquid pool relatively large bubbles are formed by evaporation at the interface, which then depart from the interface and rise up through the liquid pool.

Heat transfer coefficients on the nucleate pool boiling portion of Nukiyama's curve are much larger than those for simple natural convection to the liquid. The three principal heat transfer mechanisms thought to control the nucleate pool boiling process are illustrated in Figure 9.7 that can be explained as follows:

- ***Bubble agitation mechanism***. Intense convection in the liquid adjacent to the heated wall is induced by the lateral pumping motion of growing and departing bubbles, which transforms the natural convection process into a localized forced convection process. Sensible heat is carried away from the surface in the form of superheated liquid.

- ***Vapor-liquid exchange mechanism***. Transient conduction from the hot wall into the liquid forms a superheated layer on the surface and its removal by departing bubbles gives rise to a cyclic thermal boundary layer stripping phenomenon. Sensible heat is transported away from the surface by this mechanism, whose intensity depends on the rate of layer removal, its mean temperature, the area of influence of departing bubbles and their departure frequency, and finally the density of active boiling sites.

- ***Evaporation mechanism***. Vapor bubbles grow in the superheated layer formed on the heated surface. Macro-evaporation occurs over the top of the bubble surrounded by the thermal boundary layer while micro-evaporation occurs underneath the bubble across the thin layer of liquid trapped between a rapidly growing bubble and the surface, the latter which is often referred to as *microlayer evaporation*. Latent heat is transported by this mechanism. Since bubbles rise much faster than liquid natural convection currents and contain a large quantity of energy due to the latent heat absorbed by the bubble, this is a very efficient heat transport mechanism.

The above mechanisms are not exclusive of one another in that each is competing for the same heat. For instance, the evaporation mechanism tries to remove enthalpy from the thermal boundary layer in the form of latent heat while the other two mechanisms try to carry away the same enthalpy as sensible heat. At low heat fluxes with only isolated bubbles on the surface, natural convection occurs on the inactive areas of the surface.

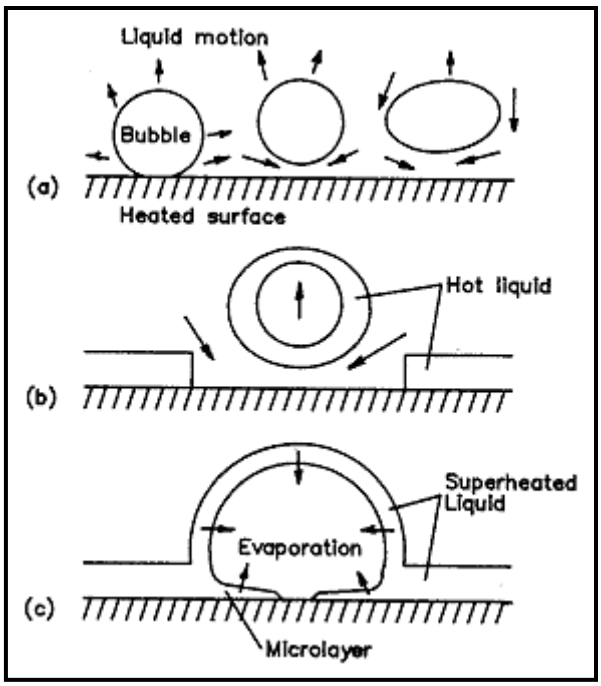

Figure 9.7. Nucleate boiling mechanisms. (a) bubble agitation, (b) vapor-liquid exchange, (c) evaporation.

9.3.2 Nucleate Pool Boiling Correlations

Experimental results for heat flux q and wall superheat ΔT are typically fit to an exponential equation of one of the following forms: $q \propto \Delta T^n$, $\alpha_{nb} \propto \Delta T^n$ or $\alpha_{nb} \propto q^n$, where n is on the order of 3, 2 or 0.7, respectively. The nucleate boiling curve is not linear at low heat fluxes nor as it approaches DNB, but these zones are often excluded (or not measured) when fitting a curve to experimental data. Nucleate pool boiling correlations can be formulated in one of the above forms but those presented as $\alpha_{nb} \propto q^n$ are the easiest to apply. Some nucleate pool boiling correlations are presented below, which are empirical representations of experimental data.

Rohsenow Correlation. Rohsenow (1962) proposed one of the first nucleate pool boiling correlations, based on the premise of the bubble agitation mechanism and formulated as a single phase forced convection correlation:

$$Nu = C_1 \, Re^x \, Pr^y \qquad [9.3.1]$$

The Nusselt number for boiling was defined as follows where the bracketed term is the bubble departure diameter, designated as the characteristic length:

$$Nu = \frac{\alpha_{nb}}{k_L}\left[\frac{\sigma}{g(\rho_L - \rho_G)}\right]^{1/2} \qquad [9.3.2]$$

In this expression, α_{nb} is the nucleate pool boiling heat transfer coefficient, k_L is the liquid thermal conductivity, σ is the surface tension, g is the gravitational acceleration, and ρ_L and ρ_G are the densities of the liquid and vapor phases. His Reynolds number was defined in terms of the superficial velocity of the liquid as

$$Re = \frac{q}{h_{LG}\rho_L}\left[\frac{\sigma}{g(\rho_L - \rho_G)}\right]^{1/2}\frac{\rho_L}{\mu_L} \qquad [9.3.3]$$

where h_{LG} is the latent heat and μ_L is the liquid dynamic viscosity. An empirical constant C_{sf} was introduced to account for the influence of the liquid-surface combination observed in his database as follows:

$$Nu = \frac{1}{C_{sf}} Re^{(1-n)} Pr^{-m} \qquad [9.3.4]$$

The Rohsenow correlation is normally presented in the following form:

$$\left[\frac{c_{pL}\Delta T}{h_{LG}}\right] = C_{sf}\left[\frac{q}{\mu_L h_{LG}}\left(\frac{\sigma}{g(\rho_L - \rho_G)}\right)^{1/2}\right]^n Pr_L^{m+1} \qquad [9.3.5]$$

The specific heat of the liquid is c_{pL} and Pr_L is the liquid Prandtl number; α_{nb} is obtained from the definition of the heat transfer coefficient, that is $\alpha_{nb} = q/\Delta T$. The values of the exponents are m=0.7 and n=0.33 (equivalent to $q \propto \Delta T^3$) for all fluids except for water for which Rohsenow recommended setting m=0. Values of C_{sf} for various surface-fluid combinations of Rohsenow and additional values proposed by Vachon, Nix and Tangor (1967) are listed in Table 9.1. This method is now mostly of "historical" value, pointing to the importance of the micro-topology of the boiling surface on nucleate boiling heat transfer.

Mostinski Correlation. Mostinski (1963) ignored surface effects and applied the principle of corresponding states to nucleate pool boiling heat transfer, correlating data as a function of the reduced pressure of the fluid p_r and its critical pressure p_{crit}. His *dimensional* reduced pressure correlation gives α_{nb} in W/m^2K as:

$$\alpha_{nb} = 0.00417 q^{0.7} p_{crit}^{0.69} F_P \qquad [9.3.6]$$

The correlation must be used with q in W/m^2 and p_{crit} in kN/m^2 (i.e. in kPa, not in N/m^2). F_P is a non-dimensional pressure correction factor that characterizes pressure effects on nucleate boiling as

$$F_P = 1.8 p_r^{0.17} + 4 p_r^{1.2} + 10 p_r^{10} \qquad [9.3.7]$$

This correlation gives reasonable results for a wide range of fluids and reduced pressures.

Table 9.1. Values of C_{sf} for Rohsenow correlation.

Liquid-surface combination	C_{sf}
n-Pentane on polished copper	0.0154
n-Pentane on polished nickel	0.0127
Water on polished copper	0.0128
Carbon tetrachloride on polished copper	0.0070
Water on lapped copper	0.0147
n-Pentane on lapped copper	0.0049
n-Pentane on emery polished copper	0.0074
Water on scored copper	0.0068
Water on ground and polished stainless steel	0.0800
Water on PTFE pitted stainless steel	0.0058
Water on chemically etched stainless steel	0.0133
Water on mechanically polished stainless steel	0.0132

Stephan-Abdelsalam Correlation. Stephan and Abdelsalam (1980) proposed four specific correlations applying a statistical multiple regression technique to the following fluid classes: water, organics, refrigerants and cryogens. Their organic fluid correlation is the most widely quoted and it is given as:

$$\frac{\alpha_{nb} d_{bub}}{k_L} = 0.0546 \left[\left(\frac{\rho_G}{\rho_L} \right)^{1/2} \left(\frac{q d_{bub}}{k_L T_{sat}} \right) \right]^{0.67} \left(\frac{h_{LG} d_{bub}^2}{a_L^2} \right)^{0.248} \left(\frac{\rho_L - \rho_G}{\rho_L} \right)^{-4.33} \qquad [9.3.8]$$

The expression to the left of the equal sign is a Nusselt number and their bubble departure diameter d_{bub} is obtained from

$$d_{bub} = 0.0146\, \beta \left[\frac{2\sigma}{g(\rho_L - \rho_G)} \right]^{1/2} \qquad [9.3.9]$$

The contact angle β is assigned a fixed value of 35° irrespective of the fluid, T_{sat} is the saturation temperature of the fluid in K, and a_L is the liquid thermal diffusivity.

Cooper Correlation. Cooper (1984) proposed a new reduced pressure form of pool boiling correlation including the surface roughness of the boiling surface as a variable:

$$\alpha_{nb} = 55 p_r^{0.12 - 0.4343 \ln R_p} \left(-0.4343 \ln p_r \right)^{-0.55} M^{-0.5} q^{0.67} \qquad [9.3.10]$$

This is a *dimensional* correlation in which α_{nb} is in W/m^2K, the heat flux q is in W/m^2, M is the molecular weight of the fluid and R_p is the surface roughness in μm. When R_p is unknown, it is set to 1.0 μm. He recommended multiplying the above heat transfer coefficient by 1.7 for horizontal copper cylinders; however, the correlation seems to be more accurate for boiling of refrigerants on copper tubes without this correction and that is the approach recommended here. The Cooper correlation covers reduced pressures from about 0.001 to 0.9 and molecular weights from 2 to 200.

Table 9.2. References values of Gorenflo (1993) with α_o in W/m^{2}K at p_{ro} = 0.1, q_o = 20,000 W/m^2 and R_{po} = 0.4 μm with p_{crit} in bar.

Fluid	p_{crit}	M	α_o
Methane	46.0	16.04	7000
Ethane	48.8	30.07	4500
Propane	42.4	44.10	4000
n-Butane	38.0	58.12	3600
n-Pentane	33.7	72.15	3400
i-Pentane	33.3	72.15	2500
n-Hexane	29.7	86.18	3300
n-Heptane	27.3	100.2	3200
Benzene	48.9	78.11	2750
Toluene	41.1	92.14	2650
Diphenyl	38.5	154.2	2100
Ethanol	63.8	46.07	4400
n-Propanol	51.7	60.10	3800
i-propanol	47.6	60.10	3000
n-Butanol	49.6	74.12	2600
i-Butanol	43.0	74.12	4500
Acetone	47.0	58.08	3950
R-11	44.0	137.4	2800
R-12	41.6	120.9	4000
R-13	38.6	104.5	3900
R-13B1	39.8	148.9	3500
R-22	49.9	86.47	3900
R-23	48.7	70.02	4400
R-113	34.1	187.4	2650
R-114	32.6	170.9	2800
R-115	31.3	154.5	4200
R-123	36.7	152.9	2600
R-134a	40.6	102.0	4500
R-152a	45.2	66.05	4000
R-226	30.6	186.5	3700
R-227	29.3	170.0	3800
RC318	28.0	200.0	4200
R-502	40.8	111.6	3300
Chloromethane	66.8	50.49	4400
Tetrafluoromethane	37.4	88.00	4750
Hydrogen (on Cu)	12.97	2.02	24000
Neon (on Cu)	26.5	20.18	20000
Nitrogen (on Cu)	34.0	28.02	10000
Nitrogen (on Pt)	34.0	28.02	7000
Argon (on Cu)	49.0	39.95	8200
Argon (on Pt)	49.0	39.95	6700
Oxygen (on Cu)	50.5	32.00	9500
Oxygen (on Pt)	50.5	32.00	7200
Water	220.6	18.02	5600
Ammonia	113.0	17.03	7000
Carbon Dioxide *	73.8	44.01	5100
Sulfur Hexafluoride	37.6	146.1	3700

* At triple point.

Gorenflo Correlation. Gorenflo (1993) proposed a fluid specific reduced pressure correlation and included the effect of surface roughness. His method uses a reference heat transfer coefficient, α_o, specified for each fluid at the following fixed reference conditions of p_{ro}=0.1, R_{po}=0.4 μm and q_o=20,000 W/m^2. His values of α_o are listed in Table 9.2 for selected fluids. The nucleate boiling heat transfer coefficient α_{nb} at other conditions of pressure, heat flux and roughness is then calculated relative to the reference heat transfer coefficient using the following expression:

$$\alpha_{nb} = \alpha_o F_{PF} (q/q_0)^{nf} \left(R_p/R_{po}\right)^{0.133} \qquad [9.3.11]$$

His pressure correction factor F_{PF} is

$$F_{PF} = 1.2p_r^{0.27} + 2.5p_r + \frac{p_r}{1-p_r} \qquad [9.3.12]$$

The effect of reduced pressure on his exponent nf for the heat flux term is given by:

$$nf = 0.9 - 0.3p_r^{0.3} \qquad [9.3.13]$$

Its value decreases with increasing reduced pressure, which is typical of experimental data. The surface roughness is R_p in μm and is set to 0.4 μm when unknown. The above method is for all fluids except water and helium; for water the corresponding equations are:

$$F_{PF} = 1.73p_r^{0.27} + \left(6.1 + \frac{0.68}{1-p_r}\right)p_r^2 \qquad [9.3.14]$$

and

$$nf = 0.9 - 0.3p_r^{0.15} \qquad [9.3.15]$$

This method is applicable over the reduced pressure range from about 0.0005 to 0.95. For fluids not listed, experimental values can be input at the reference conditions, or another correlation can be used to estimate α_o. For fluids on the list, this method gives accurate results over a very wide range of heat flux and pressure and is probably to most reliable of those presented.

Example Calculation: Determine the nucleate pool boiling heat transfer coefficient for n-pentane boiling on a polished copper surface (1.0 μm roughness) at a pressure of 1.01 bar and a heat flux of 30 kW/m^2 using the Gorenflo method.

Solution: From Table 9.2, we see that α_o = 3400 W/m^{2}K, p_{crit} = 33.7 bar and M = 72.15. Thus, p_r = p_{sat}/p_{crit}= 1.01/33.7 = 0.030 and thus

$$F_{PF} = 1.73(0.030)^{0.27} + \left(6.1 + \frac{0.68}{1-0.030}\right)(0.030)^2 = 0.677$$

and

$$nf = 0.9 - 0.3(0.030)^{0.3} = 0.795$$

Substituting these values into his heat transfer correlation:

$$\alpha_{nb} = 3400(0.677)(30000/20000)^{0.795}(1.0/0.4)^{0.133} = 3590\,W/m^2K$$

Ribatski-Siaz Jabardo Correlation. Surface roughness and material effects have been introduced into a new correlation proposed by Ribatski and Saiz Jabardo (2003) for nucleate pool boiling of halocarbon refrigerants. According them, the nucleate pool boiling heat transfer coefficient on a horizontal copper tube can be predicted as a function of reduced pressure p_r, surface roughness R_p, molecular weight M and heat flux q as:

$$\alpha_{nb} = B\left(q^{0.9-0.3p_r^{0.2}}\right) p_r^{0.45}\left[-\log(p_r)\right]^{-0.8} R_p^{0.2}\, M^{-0.5} \qquad [9.3.16]$$

The empirical constant B in this correlation accounts for wall material effects and has the following values: B=100 for copper, B=110 for brass and B=85 for stainless steel. In this dimensional correlation, the heat flux q is input in W/m^2 and the resulting nucleate boiling heat transfer coefficient α_{nb} is in W/m^2K. R_p is the arithmetic mean deviation of the surface profile as per ISO 4287/1:1984 in microns. Averaging 10 measurements from ten different areas on 10 different commercial copper tube samples, they found a mean roughness of 0.6 microns (this is thus the best value to use when its actual value is unknown). This correlation was developed based on pool boiling data for the following conditions:

- Refrigerants: R-11, R-123, R-12, R-134a and R-22;
- Reduced pressure: 0.008 to 0.260;
- Heat flux: 2.3 to 120 kW/m^2 (730 to 38000 Btu/h ft^2);
- Surface materials: copper, brass and stainless steel;
- Surface roughness: 0.02 to 3.3 microns.

Note that the exponent on the heat flux in their correlation is similar to those in [9.3.13] and [9.3.15] above whereas the exponent of -0.5 on the molecular weight M is the same as in [9.3.10]. This correlation captured most of their heat transfer data within an error band of ±20% and also worked well for some data from several other studies: R-11, R-113 and R-114 on a 14.2 mm diameter brass tube by Silva (1989) and R-113 on a 12.7 mm diameter stainless steel tube from Jensen (1985).

9.3.3 Departure from Nucleate Boiling

The maximum heat flux attainable in the nucleate pool boiling regime of the pool boiling curve illustrated in Figure 9.5 is the DNB point. This heat flux is called q_{DNB} and is also often referred to as the critical heat flux. The maximum in heat transfer rate occurs at the point of onset of a hydrodynamic instability occurring close to the heater surface, which was first explained by Zuber (1959) to be governed by the Taylor and Helmholtz instabilities. His model has since been refined by Lienhard and Dhir (1973) for an infinite surface.

The *Taylor instability* governs the collapse of an infinite, horizontal planar interface of liquid above a vapor or gas. The Taylor wavelength is that which predominates at the interface during such a collapse. In the present case at the DNB, vapor jets formed above a large, flat horizontal heater surface occur at spacings corresponding to the wavelength of the Taylor instability. The *Helmholtz instability*, instead, describes the point at which a planar liquid interface goes unstable when the velocity of a vapor or gas

flowing parallel to their interface reaches some critical value. Essentially, a small perturbation of the interface creates a low pressure zone on the convex side and a high pressure zone on the concave side. The imbalance of the opposing pressure forces acting on the vapor-liquid interface induces an instability, which is attenuated by interfacial surface tension. According to Zuber, it is the liquid interface of the rising vapor jets that go unstable. The resulting expression for q_{DNB} from such an analysis is:

$$q_{DNB} = \rho_G h_{LG} \sqrt{\frac{2\pi\sigma}{\rho_G}} \frac{1}{2\pi\sqrt{3}} \sqrt{\frac{g(\rho_L - \rho_G)}{\sigma}} \frac{\pi}{16} \qquad [9.3.17]$$

which is equivalent to

$$q_{DNB} = 0.149\, \rho_G^{1/2} h_{LG} \sqrt[4]{g(\rho_L - \rho_G)\sigma} \qquad [9.3.18]$$

This equation is valid for flat infinite heaters facing upwards. Lienhard and Dhir (1973) observed good agreement as long as the diameters or widths of the heaters were sufficiently large. Kutateladze (1948) had already arrived at nearly the same expression using dimensional analysis:

$$q_{DNB} = C\rho_G^{1/2} h_{LG} \sqrt[4]{g(\rho_L - \rho_G)\sigma} \qquad [9.3.19]$$

His empirical factor C was set to 0.131 based on comparison to experimental data. Zuber's analysis yielded a value of $C = \pi/24 = 0.1309$, which is nearly identical to Kutateladze's value. The Lienhard and Dhir solution for an infinite flat surface facing upwards gives $C = 0.149$, which is 15% higher. The recommended expression for large surfaces is $C = 0.1309$ while for tubes this value is corrected by a factor of 0.9. Refer to Collier and Thome (1994) for a description of the methods proposed by Lienhard and Dhir for specific geometries.

Example Calculation: Determine the value of the heat flux at the DNB for water at 1.01 bar on a horizontal tube where the required fluid physical properties are: $\rho_L = 958.25$ kg/m^3; $\rho_G = 0.6$ kg/m^3; $h_{LG} = 2256120$ J/kg; $\sigma = 0.05878$ N/m.

Solution: The value of q_{DNB} is first calculated and then that for the tube applying a correction of 0.9 as follows:

$$q_{DNB,tube} = 0.9(\pi/24)(0.6)^{1/2}(2256120)\sqrt[4]{9.81(958.25-0.6)(0.05878)}$$
$$q_{DNB,tube} = 998100 \text{ W/m}^2$$

Therefore, the heat flux at DNB for the tube is 998100 W/m^2 (or 998.1 kW/m^2).

9.4 Nucleate Boiling of Mixtures

Nucleate pool boiling of zeotropic mixtures is similar to boiling of pure fluids and azeotropic mixtures, except for two additional complications: mass transfer effects and estimating the mixture physical properties or the mixture critical pressure. Mass transfer occurs in evaporation of *zeotropic* mixtures since they have different compositions in their liquid and vapor phases, but not *azeotropic* mixtures since they have the same composition in each phase. Mass transfer tends to reduce nucleate boiling heat transfer coefficients and, in some cases, may reduce the value of the heat transfer coefficient by up to 90%.

Detailed reviews of mixture boiling are given by Thome and Shock (1984) and by Collier and Thome (1994).

The mass transfer effect on bubble growth can be explained in simple terms as follows. Since the equilibrium composition of the more volatile component is larger in the vapor phase than in the liquid phase, the more volatile component preferentially evaporates at the bubble interface, which in turn reduces its composition there and induces the formation of a diffusion layer in the liquid surrounding the bubble. The partial depletion of the more volatile component at the interface increases that of the less volatile component, which increases the bubble point temperature at the interface. This incremental rise in the local bubble point temperature can be denoted as $\Delta\theta$. Hence, to evaporate at the same rate as in a pure fluid, a larger superheat is required for a mixture.

The effect of mass transfer on nucleate pool boiling heat transfer can therefore be explained by introducing the parameter $\Delta\theta$, which represents the increase in the bubble point temperature at the surface due to preferential evaporation of the more volatile component. At a given heat flux, the boiling superheat of the mixture is $\Delta T+\Delta\theta$ while that for an ideal fluid with the same physical properties as the mixture is ΔT_I. Thus, the ratio of the mixture boiling heat transfer coefficient α_{nb} to that of the ideal heat transfer coefficient $\alpha_{nb,I}$ at the same heat flux is:

$$\frac{\alpha_{nb}}{\alpha_{nb,I}} = \frac{\Delta T_I}{\Delta T_I + \Delta\theta} \qquad [9.4.1]$$

The value of ΔT_I is the wall superheat that corresponds to $\alpha_{nb,I}$, which is determined for instance using the Cooper correlation with the molecular weight and critical pressure of the mixture. Hence, as the value of $\Delta\theta$ increases, the ratio $\alpha_{nb}/\alpha_{nb,I}$ decreases, which means that a larger wall superheat is required in a mixture to transfer the same heat flux. As exploited in an early mixture boiling prediction by Thome (1983), the maximum value of $\Delta\theta$ is the boiling range of the mixture $\Delta\theta_{bp}$, which is equal to the difference between the dew point and the bubble point temperatures at the composition of the liquid [$\Delta\theta_{bp}$ is also referred to as the temperature glide for refrigerant mixtures]. In fact, the actual value of $\Delta\theta$ varies from zero at the inception of boiling, since no mass transfer occurs until evaporation takes place, up to $\Delta\theta_{bp}$ at the DNB, where all the liquid is assumed to be converted to vapor. Starting from a mass transfer balance around an evaporating bubble and simplifying with an approximate slope of the bubble point curve, the following expression was obtained to predict heat transfer in the boiling of mixtures

$$\frac{\alpha_{nb}}{\alpha_{nb,I}} = \left\{1 + \frac{\alpha_{nb,I}}{q}\Delta\theta_{bp}\left(1 - \exp\frac{-q}{\rho_L h_{LG}\beta_{mL}}\right)\right\}^{-1} \qquad [9.4.2]$$

where β_{mL} is the mass transfer coefficient in the liquid (set to a fixed value of 0.0003 m/s). The value of $\alpha_{nb,I}$ is determined with one of the pure fluid correlations presented earlier (with the exception of the Gorenflo method that is not adapted to this). This method was proposed in 1985 and later published by Thome (1989). It is applicable to organic, refrigerant, aqueous, hydrocarbon, and cryogenic multi-component mixtures (i.e. with two or more components) for boiling ranges up to 30 K.

Example Calculation: Assuming an ideal heat transfer coefficient of 3000 W/m^{2}K, determine the mixture boiling coefficient at 50 kW/m^2 for a mixture with a boiling range of 15 K, a liquid density of 700 kg/m^3 and a latent heat of 300000 J/kg.

Solution: Substituting values into the above expression,

$$\frac{\alpha_{nb}}{3000} = \left\{1 + \frac{3000}{50000}(15)\left(1 - \exp\frac{-50000}{700(300000)(0.0003)}\right)\right\}^{-1} = 0.670$$

$$\alpha_{nb} = 0.67(3000) = 2009\ \mathrm{W/m^2K}$$

Thus, α_{nb} for the mixture is 2009 W/m^{2}K, which is 33% lower than that of the equivalent pure fluid.

9.5 Boiling on Enhanced Tubes

Boiling heat transfer coefficients on smooth surfaces can be increased by roughening the surface, but this is not normally practical (and perhaps temporal if the surface fouls). To achieve significant enhancement, numerous types of geometries have been proposed and patented. The earliest commercial enhancement was the integral low finned tube, with its continuous helical fins around the circumference of the tube. Tubes with external porous coatings were apparently the next important enhancement to be proposed, yielding augmentations of up to 10-15 times the boiling performances on plain tubes at optimum conditions. In recent years, attention has been nearly entirely focused on mechanically deformed low finned tubes, whose fins can be notched, knurled, bent and/or compressed to form a high density of re-entrant channels and boiling pores, geometries that essentially mechanically emulate a porous coating.

9.5.1 Heat Transfer Mechanisms

Compared to a plain tube, enhanced nucleate boiling surfaces have significant performance advantages. For instance, the enhancement ratio at the same wall superheat relative to that of a comparable plain tube range from about 2-4 for low finned tubes but increase up to 15 times for mechanically deformed low finned tubes such as for the Turbo-B tubes of Wolverine Tube Inc. Evaporation and convection occur both on the outside surface of an enhanced boiling surface and inside its re-entrant passageways. Hence, as illustrated in Figure 9.8, there are four possible paths by which heat can leave an enhanced surface:

1. As latent heat in vapor formed within the enhancement passageways (primary importance);
2. As latent heat in bubbles growing on exterior of tube or while they are emerging from re-entrant channels (secondary importance);
3. As sensible heat to liquid “pumped” through the re-entrant passageways (primary importance);
4. As sensible heat to liquid on external of tube (secondary importance).

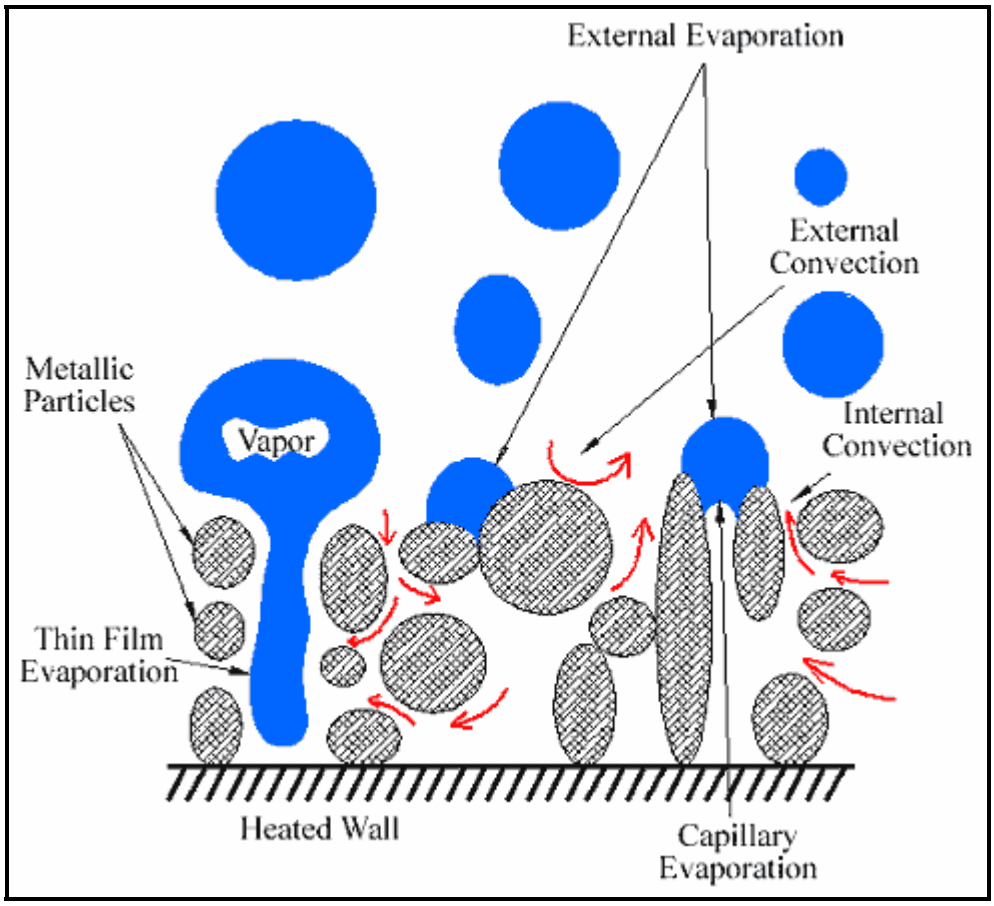

Figure 9.8. Boiling mechanisms on an enhanced surface tube.

The principal factors contributing to the high thermal performance of enhanced surfaces have been identified by Thome (1990) as follows:

- ***Nucleation superheat***. Enhanced surfaces have re-entrant nucleation cavities (except for low finned tubes) that are able to nucleate at very low wall superheats with respect to plain surfaces, see Figure 9.9.

- ***Wetted surface area***. Low finned tubes have from 2 to 4 times the surface area of a plain tube while complex enhancements have area ratios from 4 to 10 times those of plain tubes.

- ***Thin film evaporation***. Thin evaporating liquid films form on the extensive inner surfaces of the re-entrant passageways.

- ***Capillary evaporation***. In corners, liquid menisci evaporate as heat is conducted into the liquid behind them.

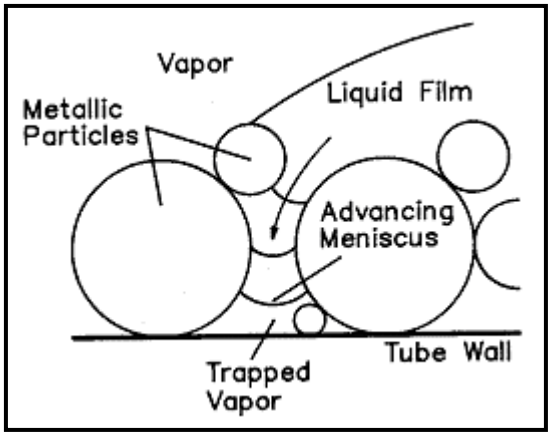

Figure 9.9. Boiling nucleation on an enhanced surface.

- ***Internal convection***. Liquid is pumped in and then back out of the re-entrant channels by the action of the departing bubbles.

- ***External convection***. The high density and departure frequency of the bubbles emerging from the re-entrant channels accentuates the external convection mechanisms, i.e. bubble agitation and thermal boundary layer stripping.

These mechanisms can be compared to those occurring on a plain surface discussed earlier. The thermal effectiveness of these factors depends on the type of enhanced surface geometry and its characteristic dimensions.

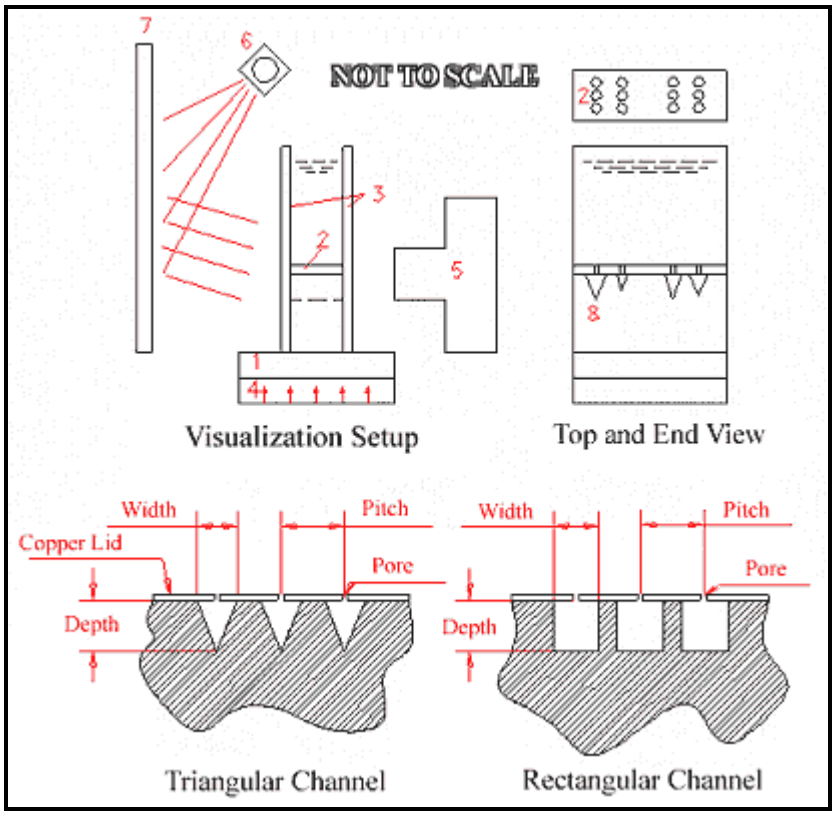

Figure 9.10. Setup of Arshad and Thome (1983) for flow visualization in re-entrant channels [1-base block with microgrooves, 2-copper sheet with pores, 3-glass walls, 4-heater, 5-camera, 6-lighting, 7-reflection panel, 8-end view of microgrooves].

The formation of liquid films inside re-entrant channels was originally investigated visually by Nakayama et al. (1979) using side channel walls made of glass. They observed that elongated bubbles formed within the re-entrant channel with thin liquid films covering the walls, particularly in the corners (they had a side view of the process). They noted pulsation of the liquid film upon departure of bubbles from the pores connecting the channels to the exterior.

In a similar study, but with an end (cross-sectional) view of the process in re-entrant channels of circular, triangular and rectangular shape, Arshad and Thome (1983) used a motor driven still camera to observe the formation and dryout of the thin liquid films. Figure 9.10 shows their experimental setup and Figure 9.11 shows some of their photographs of the process. Figure 9.12 illustrates a schematic sequence of nucleation, formation and dryout of a liquid film in a triangular re-entrant channel upon application of a high heating rate. Figure 9.13 illustrates a thin film evaporation model hypothesized by Xin and Chao (1985) for rectangular re-entrant channels with a slit opening. Hence, thin evaporating films were seen to be an important heat transfer mechanism, analogous to the microlayers formed underneath rapidly growing bubbles on plain surfaces, and are active over a large surface area. Refer to Thome (1990) for a comprehensive treatment of this subject.

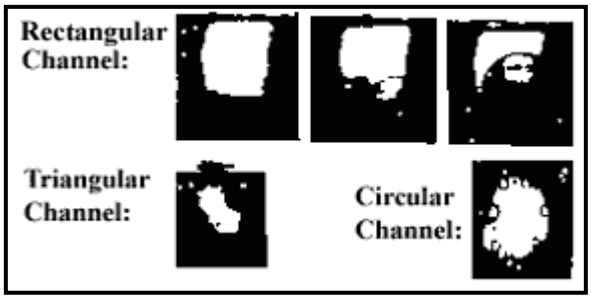

Figure 9.11. Photographs of liquid thin film formation in re-entrant channels.

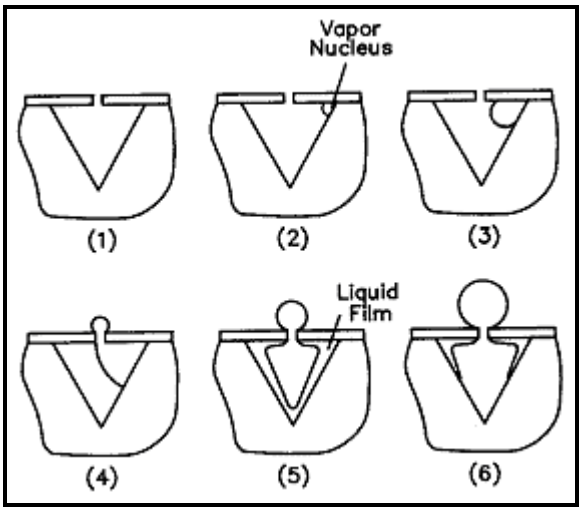

Figure 9.12. Schematic representation of films observed in a triangular re-entrant channel.

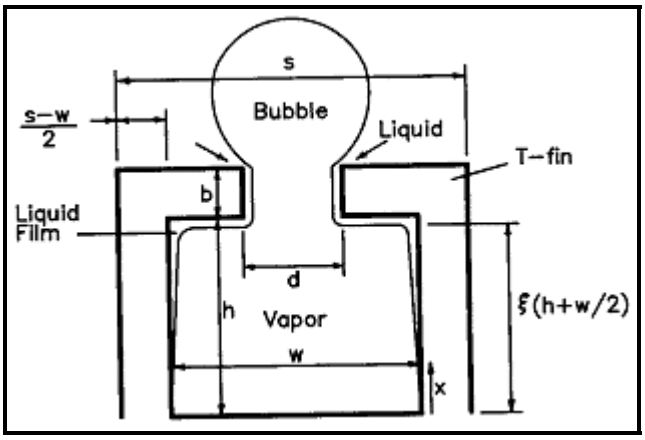

Figure 9.13. Thin film evaporation process in a rectangular re-entrant channel.

9.5.2. Enhanced Boiling Results

Experimental results for enhanced boiling surfaces are shown in this section. For an example of relative performance of five refrigerants on a 26 fpi (1024 fins per meter) low finned tube, Figure 9.14 presents the results obtained by Webb and Pais (1992). The boiling performance of R-123 was observed to be similar to that of R-11 while the three higher saturation pressure refrigerants had significantly higher heat transfer coefficients.

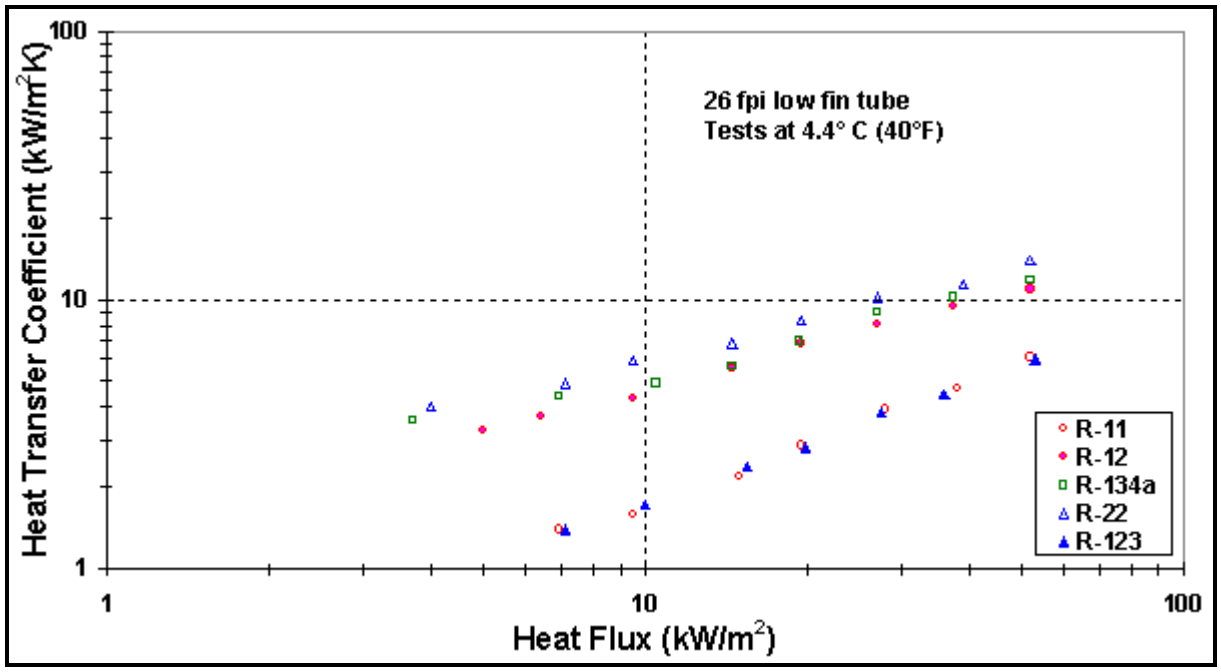

Figure 9.14. Pool boiling of five refrigerants on a low finned by Webb and Pais (1992).

Figure 9.15 shows the nucleate pool boiling results for a low finned tube and a Turbo-B tube compared to a plain tube obtained by Palm (1995) for R-134a at 0.7°C (33.3°F) and R-22 at 0.1°C (32.2°F), albeit plotted in a linear form as in the original publication. The boiling curves illustrate that the most important enhancement factor at a fixed wall superheat is obtained at low superheats.

Figure 9.16 shows some pool boiling results for a Turbo-B tube compared to those for a plain tube for R-123 at 4.4°C (40°F) by Webb et al. (1995). Significant boiling enhancement is evident over the entire heat flux range.

Figure 9.17 depicts some other pool boiling for a Turbo-Bii-LP tube for R-123 at 4°C (39°F) taken by Kedzierski (1995) and compared to a low finned tube. They plotted their data on a linear graph as reproduced here. They took a large number of data points with little scatter as can be noted.

Figure 9.18 presents the pool boiling heat transfer coefficients plotted versus heat flux for a Turbo-Bii tube for pure fluids (R-22 and R-134a), a near azeotrope mixture of R-32/R-125 (60/40%) and several zeotropic mixtures by Chen and Tuzla (1996). Note that the mass transfer effect has a very detrimental effect on the boiling performance for the two zeotropic mixtures.

Ribatski and Thome (2006) recently completed a comparative study on four commercially available enhanced tubes (a porous coated tube, two enhanced boiling tubes and an enhanced condensation tube) for R-134a, covering the effect of saturation temperature with tests at 5, 10 and 20°C (41, 50 and 68°F) over heat fluxes from 20 to 70 kW/m^2 (6340 to 22190 Btu/h ft^2). They also provide an extensive list of about 23 other enhanced pool boiling studies completed since 2000 for those interested. Since it may be beneficial to simplify system construction by using the same enhanced tube in both a refrigeration system's flooded evaporator as in its condenser, pool boiling tests were also done with an enhanced condensing tube to look at this possibility. Their results for two such tubes, one enhanced boiling and one enhanced condensation, are shown in Figure 9.19. The data show that there is some effect of saturation temperature on boiling performance and also that at high heat fluxes the enhanced condensing tube

actually outperforms, by a small margin, the enhanced boiling tube whereas being much less effective at lower heat fluxes.

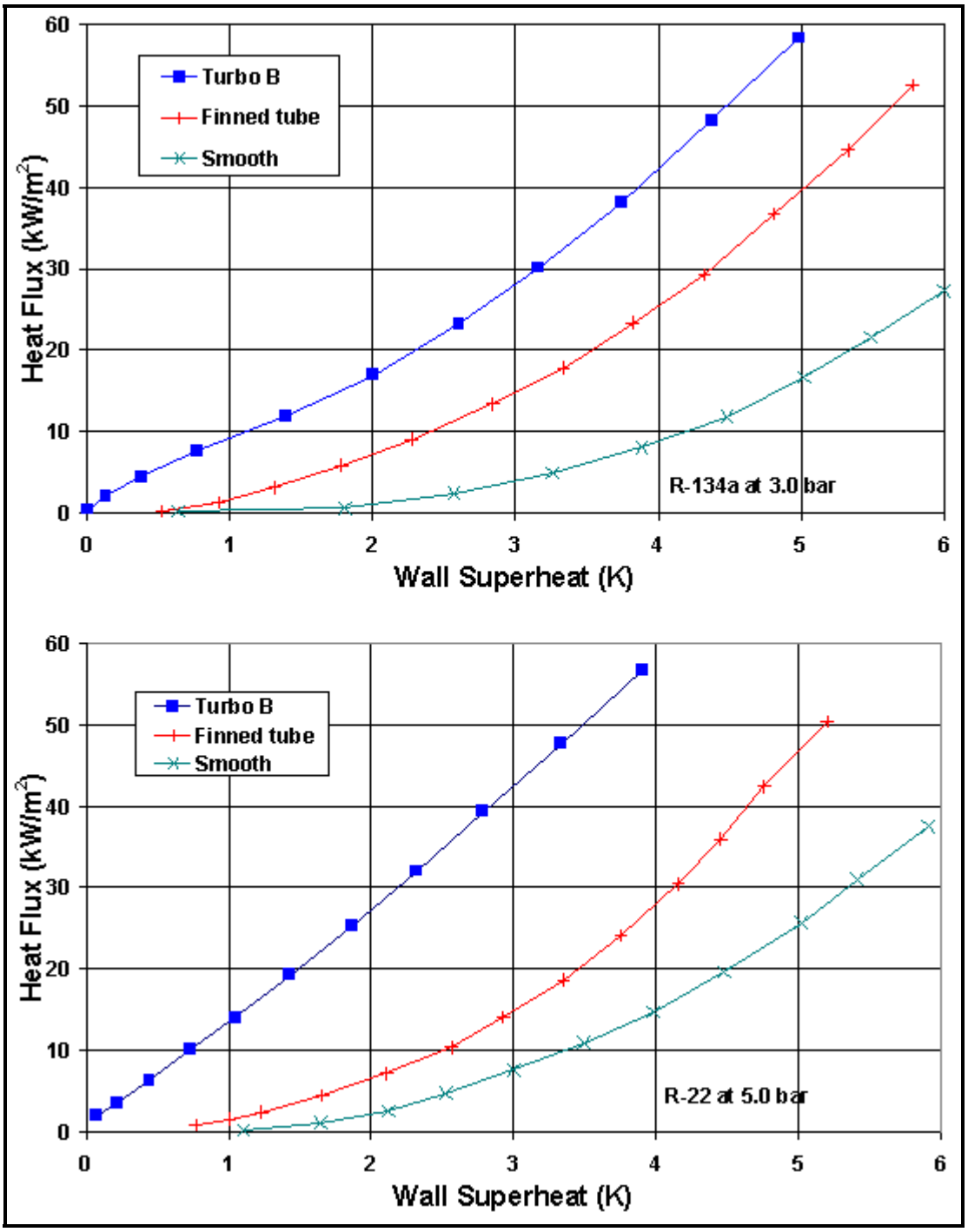

Figure 9.15. Pool boiling of R-22 and R-134a on plain, low finned and Turbo-B tubes by Palm (1995).

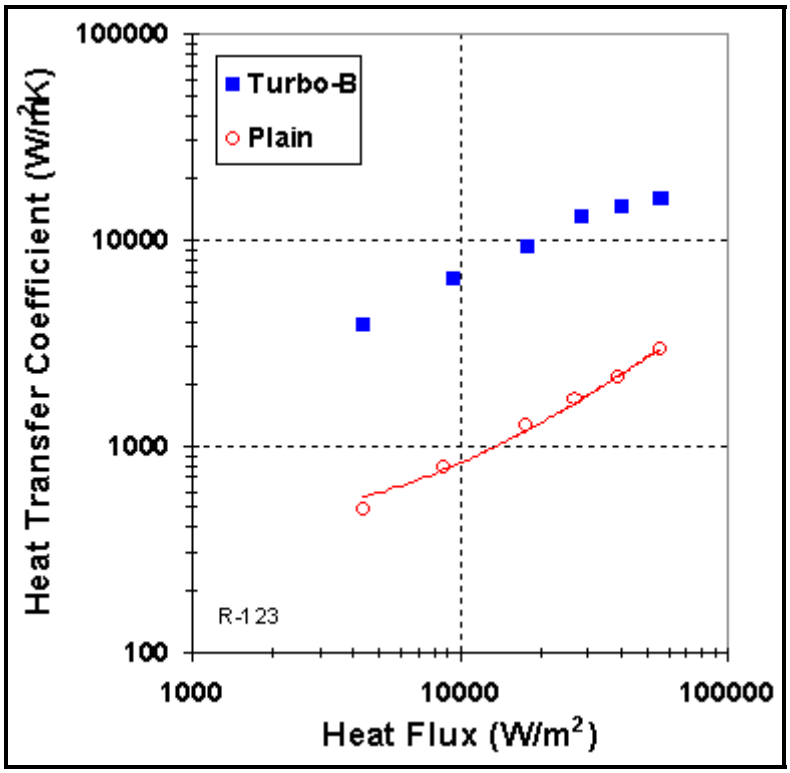

Figure 9.16. Pool boiling on a Turbo-B tube for R-123 by Webb et al. (1995).

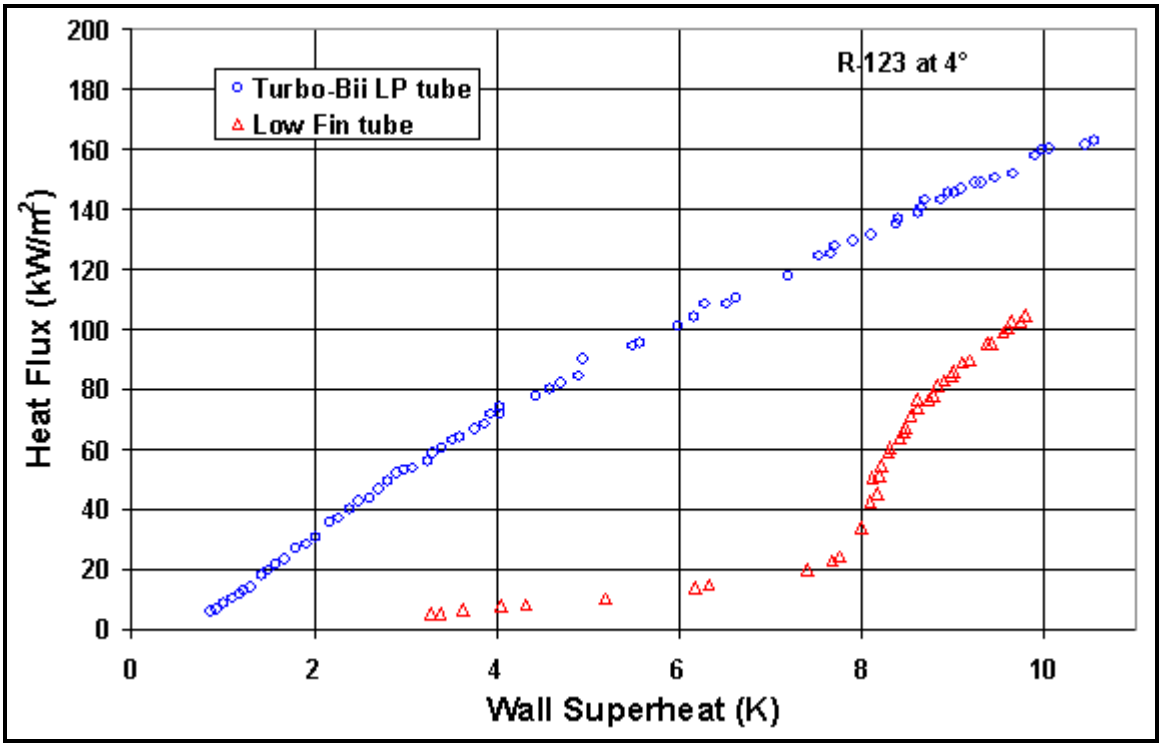

Figure 9.17. Pool boiling on Turbo-Bii-LP tube for R-123 by Kedzierski (1995).

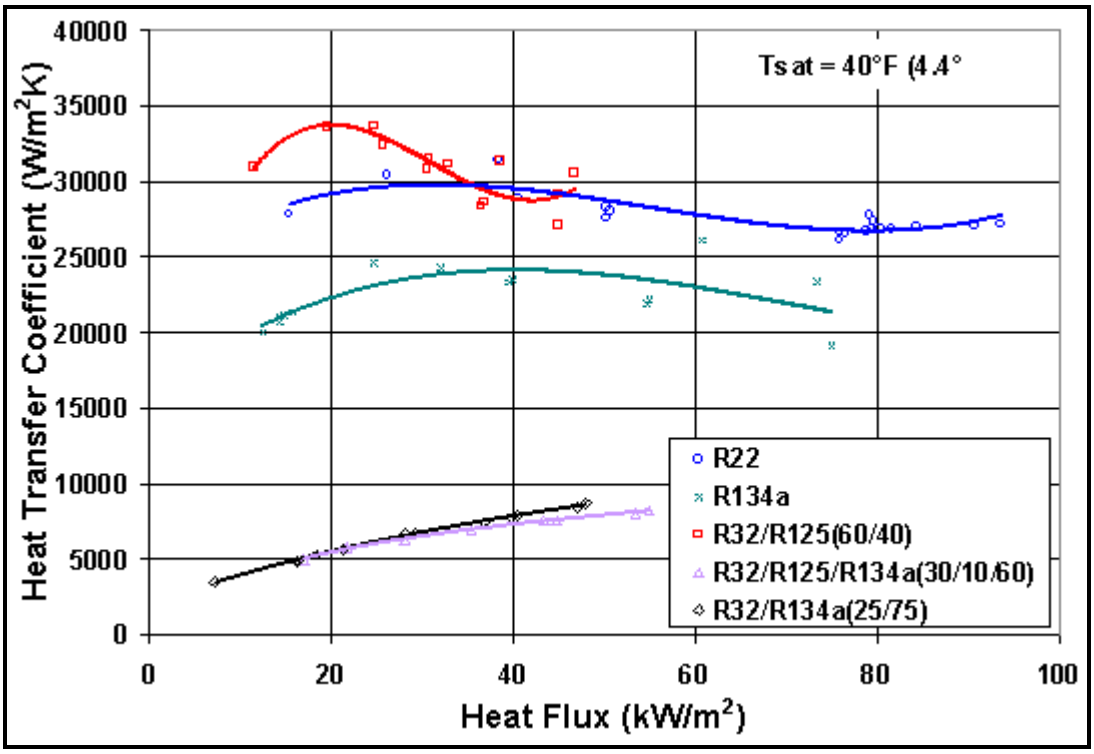

Figure 9.18. Pool boiling on Turbo-Bii for pure fluids and mixtures by Chen and Tuzla (1996).

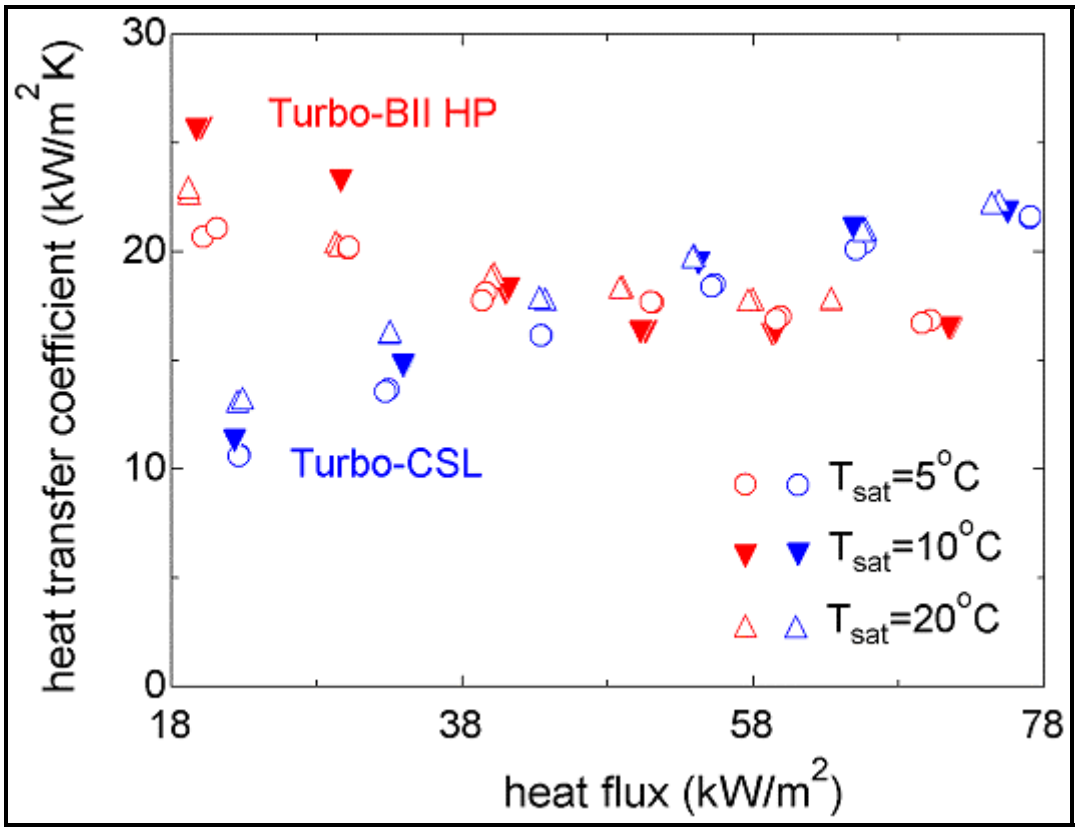

Figure 9.19. Pool boiling results for R-134a on Turbo-BII HP (boiling tube) and Turbo-CSL (condensing tube) at three saturation pressures from Ribatski and Thome (2006).

9.6 Bundle Boiling

An important heat transfer process is evaporation on the outside of horizontal tube bundles. This process is generic to refrigerant flooded evaporators, waste heat boilers, fire-tube steam generators, kettle and thermosyphon reboilers, feed effluent heat exchangers, etc. Nearly all the research has focused either on overall bundle boiling data, on mean measurements for selected tubes in the bundle, on bundles immersed in a pool of liquid without measurement of liquid flow rates or on idealized small bundles. Some such exchangers operate in simple vertical upward cross-flow, like flooded evaporators, but others are configured with as single-segmental baffled heat exchangers where the main flow is horizontal crossflow with all the associated problems of leakage streams like in similar single-phase flows. Hence, much still remains to be accomplished on the subject of bundle boiling but fortunately some of what we know about intube evaporation can be applied *qualitatively* to this external flow process. One recent review has been presented by Casciaro and Thome (2001a, 2001b), describing the state-of-the-art with respect to heat transfer, void fractions, flow patterns and maps and two-phase pressure drops with respect to evaporation on tube bundles. Thome (1998) has also summarized the bundle boiling experiments conducted in the 1990's up to that point in time. Jensen (1988) has also presented a detailed state-of-the-art review of boiling on plain tube bundles while Thome (1990) described numerous enhanced tests up to that date.

Figure 9.20 taken from Collier and Thome (1994) depicts a simplified tube bundle layout with uniform heating of the tube for upflow boiling. The flow regimes are shown in schematic form encountered from the bottom to the top, together with the corresponding heat transfer regimes. This is a composite diagram

and not all these flow regimes are necessarily encountered depending on the operating conditions. Here, it is assumed that subcooled liquid enters the bottom from the inlet nozzle and flows upward to the bottom tube row. Hence, the initial heat transfer process is single-phase convection to the subcooled liquid that is followed by subcooled boiling until the liquid reaches its saturation temperature. For example, in a thermosyphon reboiler it is common for the liquid head to impose several degrees of subcooling on the fluid entering. For enhanced tubes, this condition would be particularly acute since they are not effective for single-phase heating nor subcooled boiling. In the lower part of the bundle, bubbly flow then exists up until the transition to bubble jet flow between the tubes. The flow then enters a chugging type of flow regime with large bubbles and liquid slugs populated with numerous small bubbles. Then at some critical condition, the flow transforms into a spray flow with large droplets impinging on the tubes to form thin liquid films. Dryout (not shown) can also occur with very poor heat transfer similar to intube evaporation. With a small amount of oil present in refrigerants, it is also possible to form a frothy flow or foam. It is unlikely that all the liquid is evaporated without carryover and hence normally either a demister pad or a large oversized shell is used to separate the liquid droplets from the outgoing vapor. Figure 9.21 shows a similar diagram from Robinson and Thome (2004a) illustrating this process in a 20-tube test section they used to investigate local flow boiling heat transfer coefficients. The details of the actual process are still not well understood and the above is primarily an intuitive description.

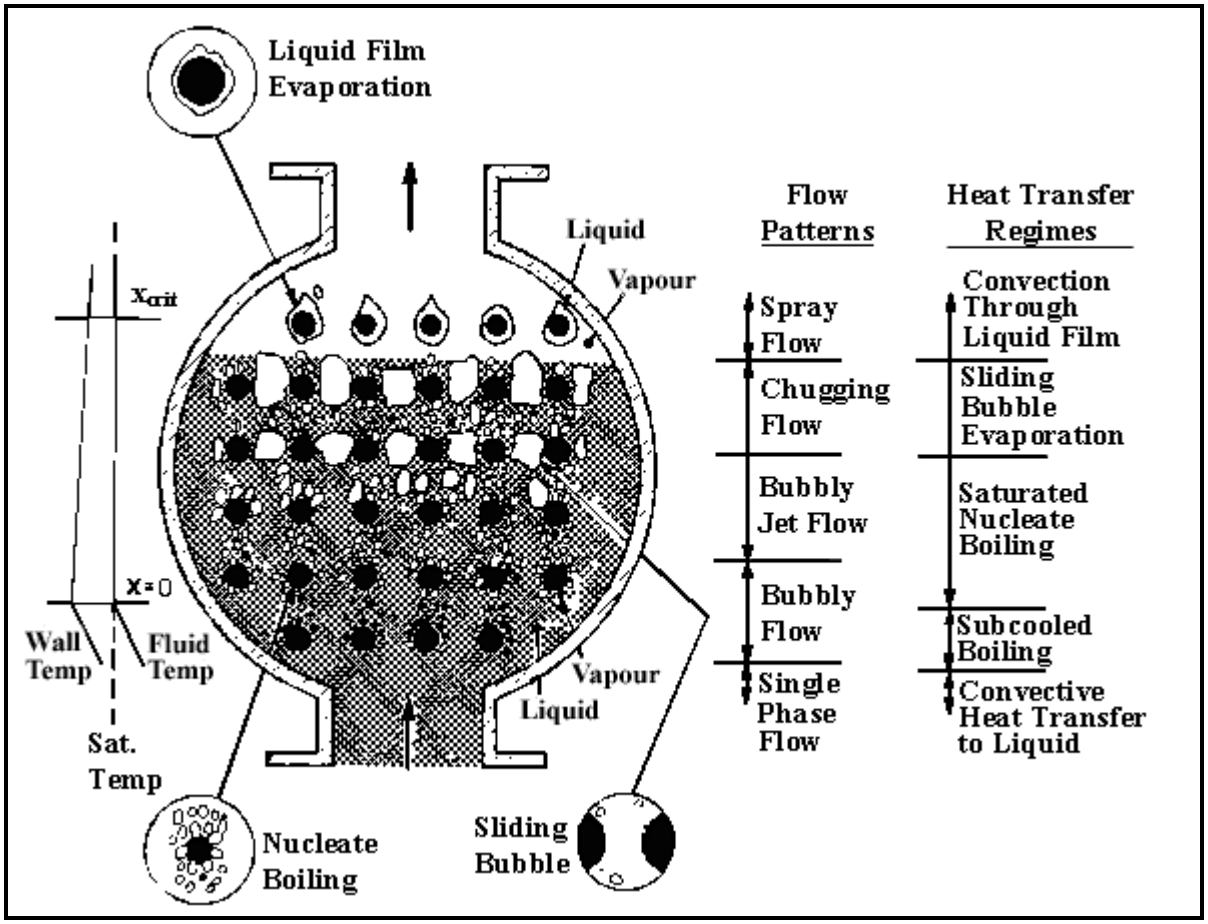

Figure 9.20. Evaporation on a horizontal tube bundle (not to scale).

Older test results in the literature are primarily for overall bundle boiling heat transfer coefficients, which are not very useful since they do not allow local boiling heat transfer models to be developed. Similarly, numerous tests on small tube bundles have been run using electrical cartridge heaters inside the tubes in

which the bundle was immersed in a large pool of liquid; hence local tube-wise heat transfer coefficients were measured but not the liquid flow rate into the bundle. Consequently, the local vapor quality cannot be determined for these test conditions, which renders these data difficult to use for building of bundle boiling models. In recent years, it has become common to run tests with complete control of the process, such that local tube-wise heat transfer coefficients have been obtained as a function of heat flux, vapor quality and mass velocity using electrical-heated or water-heated test sections.

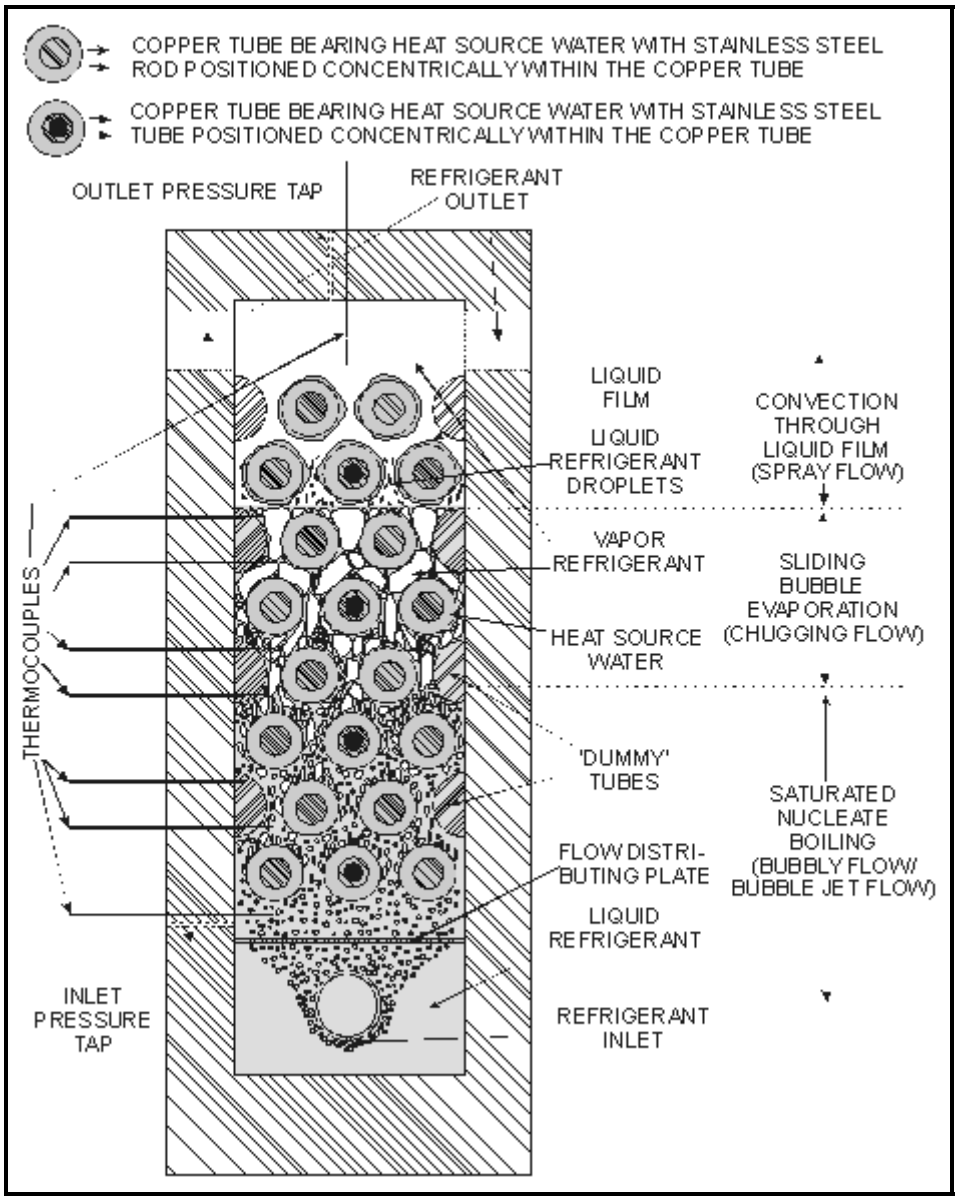

Figure 9.21. Schematic diagram of boiling in a 20-tube test section.

For boiling on the 20-tube test bundle illustrated in Figure 9.21, Robinson and Thome (2004a) used hot water heating with a modified-Wilson plot technique for their tests. They also placed dummy tubes inside the heat transfer tubes in order to install two local thermocouples inside the tubes at three locations along the four central tube rows in their bundle, besides measuring the inlet and outlet water temperatures from each tube. Hence, applying an enthalpy profile approach using the temperatures at all these locations, they were able to calculate the local heat flux at 12 locations in the bundle where the local water temperatures

have been simultaneously measured. The local refrigerant-side saturation temperatures were measured using 3 sets of an 8 thermocouple array located at the same axial position along the bundle as the internal water temperature measurements, or can be calculated from differential pressure measurements. Hence, knowing the temperatures of the water and refrigerant at any one of these locations, knowing the heat flux at that point, knowing the water-side heat transfer coefficient from the prior modified-Wilson plot tests, and the tube geometry and wall thermal conductivity, it is possible to determine the local axial flow boiling heat transfer coefficient in the bundle at known conditions of mass velocity, vapor quality and heat flux, similar to intube flow boiling test results. Their test setup hence provides 12 perimeter-averaged local heat coefficients within their tube bundle. The inlet flow conditions to the bundle are changed using a speed controlled pump and a preheater, which allows a wide range of local test conditions to be achieved within the tube bundle.

Figure 9.22 depicts some of the local bundle boiling data for R-134a on a plain tube bundle obtained by Robinson and Thome (2004a) for their tube bundle using 19.05 mm (3/4 in.) tubes on a triangular tube pitch of 22.23 mm (7/8 in.). The effect of heat flux was found to be more dominant than originally expected while the influence of mass velocity was less than expected. The local heat transfer coefficients tend to increase with local vapor quality and are larger than the corresponding nucleate pool boiling heat transfer coefficient. These data are currently being used to develop a local flow boiling heat transfer model that will be reported on in the near future.

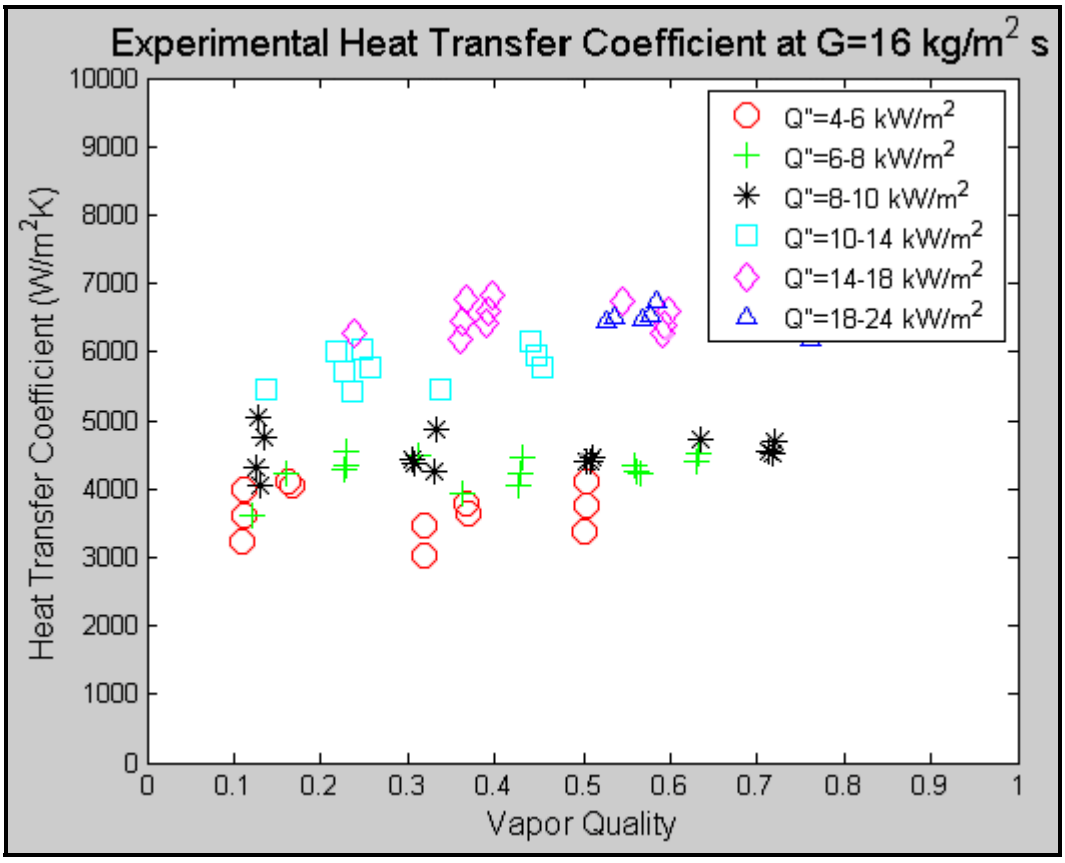

Figure 9.22. Local bundle boiling data for R-134a on a plain tube bundle of Robinson and Thome (2004a).

Figure 9.23 shows the local boiling data for R-11 evaporating on an 18.9 fpi (744 fins per meter) low fin tube bundle tested by Gupte and Webb (1995a) at 4.4°C (40°F). They used cartridge heaters to impose a

uniform heat flux in the bundle, a preheater to control the inlet vapor quality and a pump to control the refrigerant flow rate. Also indicated on the graph are the corresponding nucleate pool boiling heat transfer coefficients at the same heat fluxes. Significant convective boiling heat transfer is evident in these data with local bundle boiling coefficients up to nearly three times the nucleate pool boiling values, particularly at low heat flux.

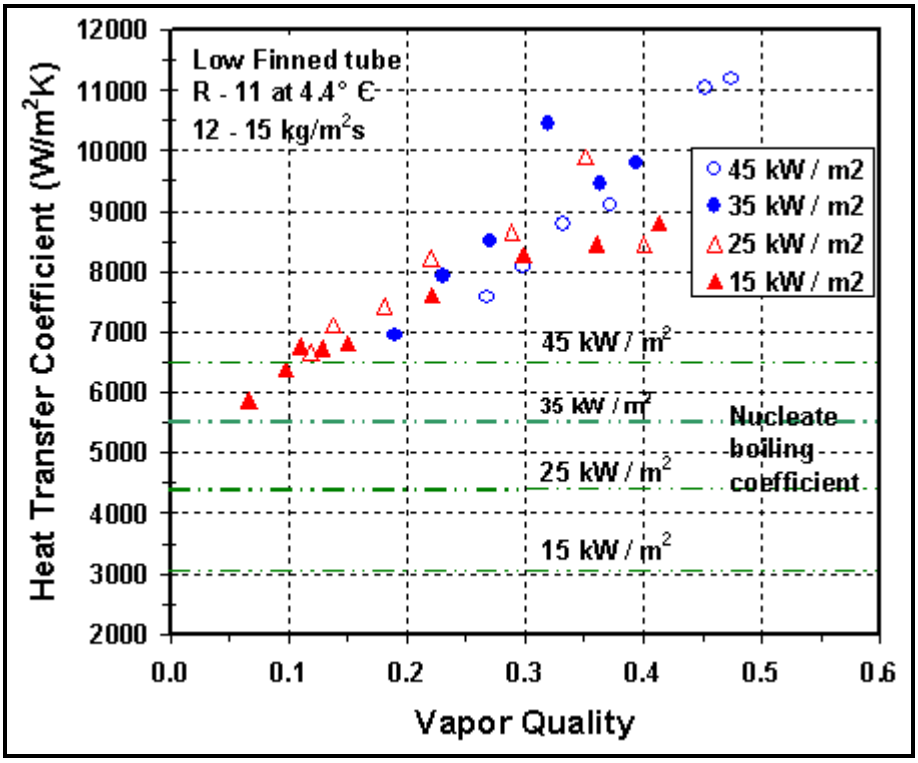

Figure 9.23. Boiling of R-11 on a 18.9 fpi low fin tube bundle by Gupte and Webb (1995a).

Figure 9.24 depicts the corresponding data of Gupte and Webb (1995a) for boiling of R-11 at a higher pressure (26.7°C or 80°F) on the same low fin tube bundle. Here, a noticeable effect of heat flux on the data is evident at the lower vapor qualities since at nucleate pool boiling is much stronger at this higher pressure. At high vapor qualities, the data tend to come together like what happens in intube flow boiling tests, suggesting that the flow is convection dominated at high vapor qualities.

Figure 9.25 shows the bundle boiling data obtained for n-pentane evaporating on 45-tube, 30 fpi low fin tube bundle by Thonon, Roser and Mercier (1997). It was not easy to distinguish the heat fluxes of individual data points on their graph, but it has been reproduced here to illustrate the significant convective effect they also observed for boiling on a low finned tube bundle at a mass velocity typical of normal operating conditions.

Figure 9.26 presents boiling data for R-123 at 4.4°C (40°F) on a Turbo-B tube bundle by Gupte and Webb (1995b) for the same bundle configuration used for their low fin tests described above. Here, they obtained data only at low vapor qualities and found little convective effect on the local boiling heat transfer coefficients, although at the lowest heat flux there appears to be the beginning of such a convective trend.

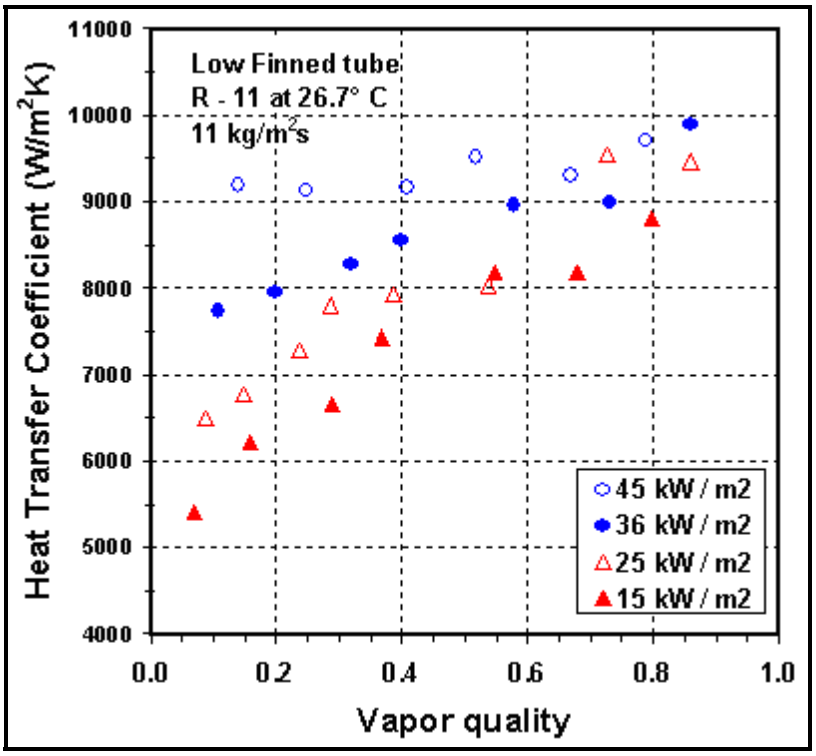

Figure 9.24. Boiling of R-11 on a 18.9 fpi low fin tube bundle by Gupte and Webb (1995a).

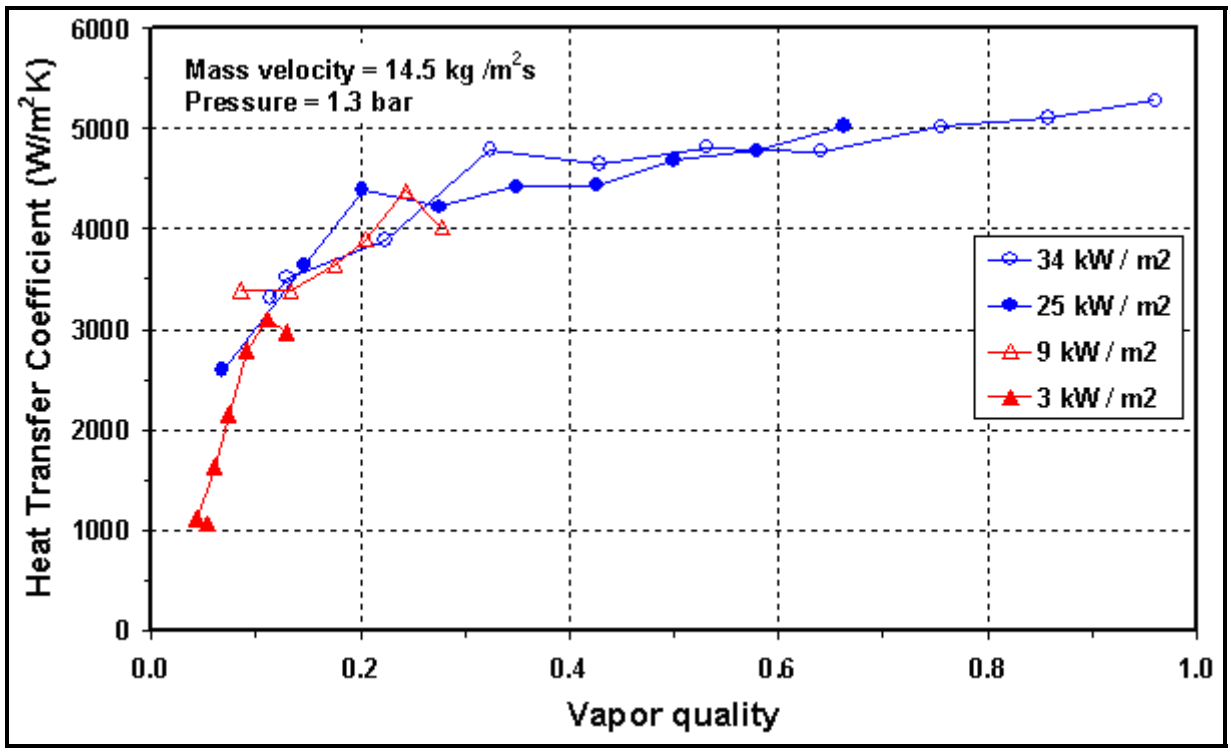

Figure 9.25. Boiling of n-pentane on a 30 fpi low fin tube bundle by Thonon, Roser and Mercier (1997).

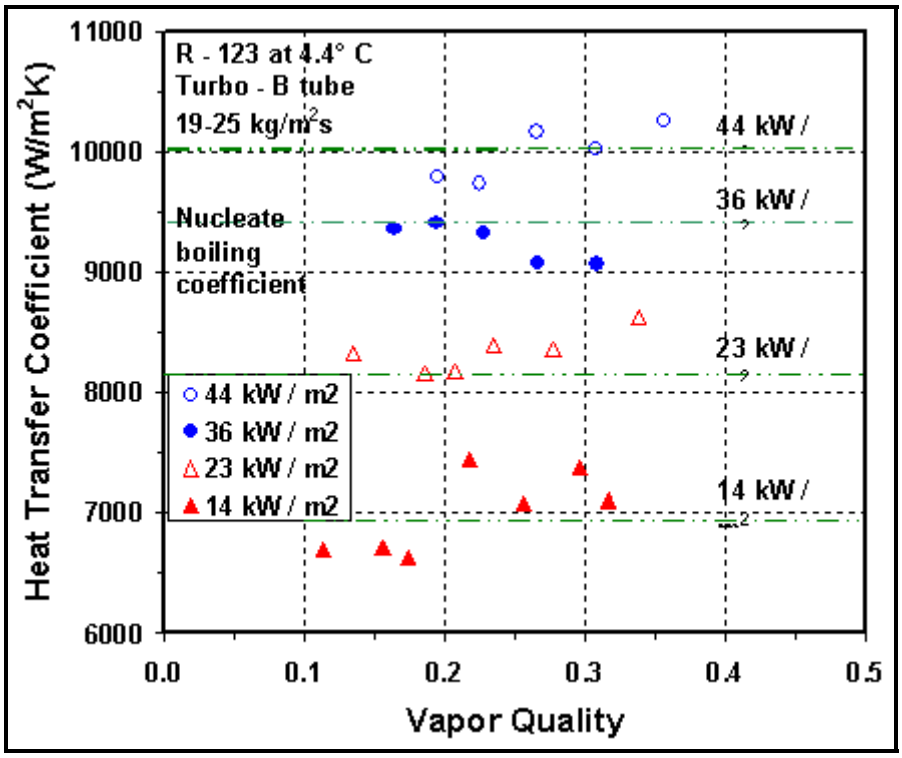

Figure 9.26. Boiling of R-123 on Turbo-B tube bundle by Gupte and Webb (1995b).

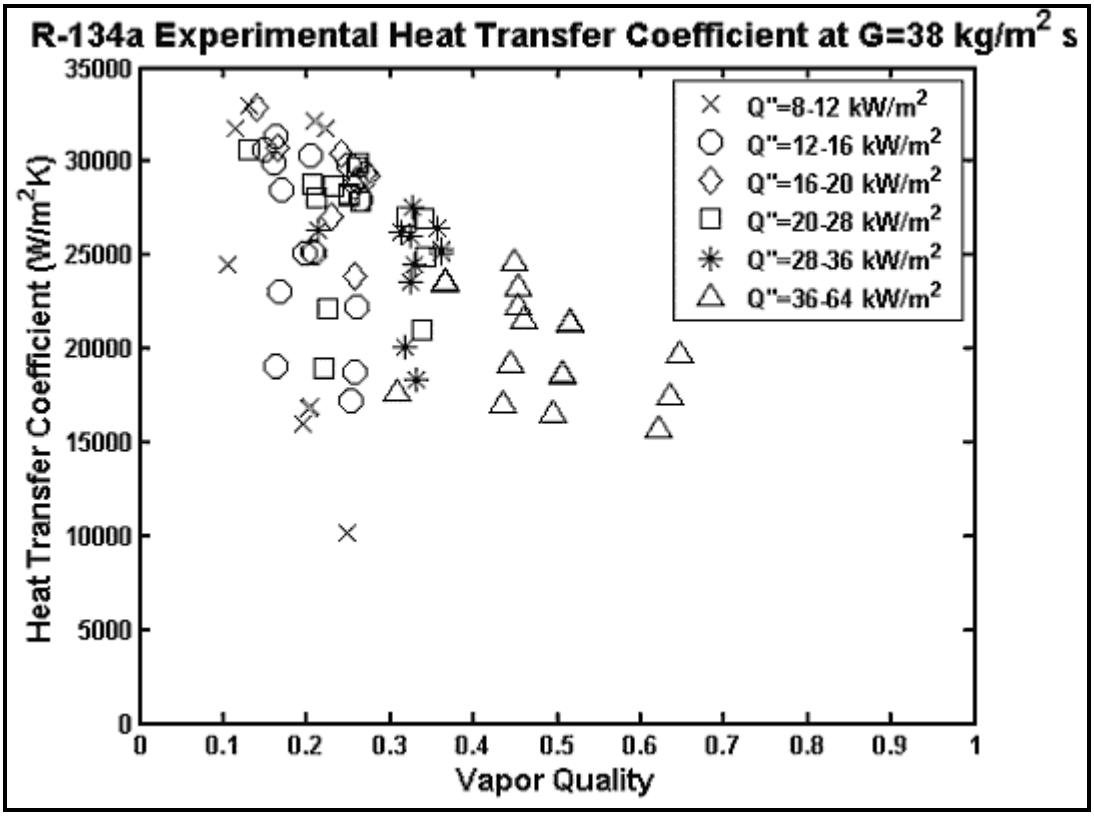

Figure 9.27. Boiling of R-134a on Turbo-Bii tube bundle by Robinson and Thome (2004b).

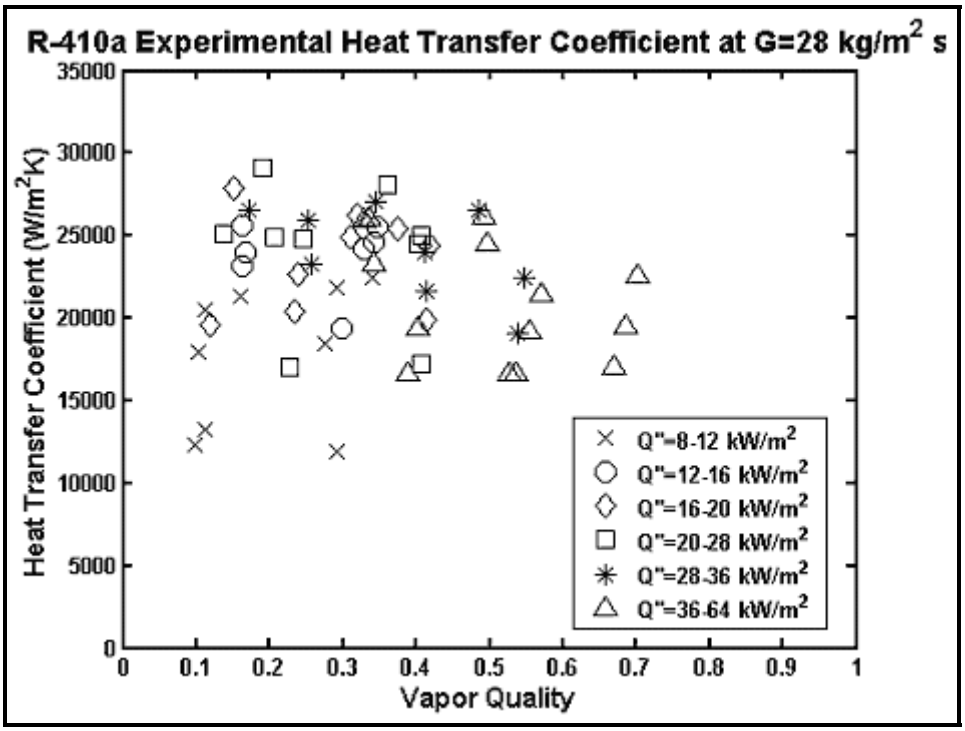

Figure 9.28. Boiling of R-410A on Turbo-Bii tube bundle by Robinson and Thome (2004b).

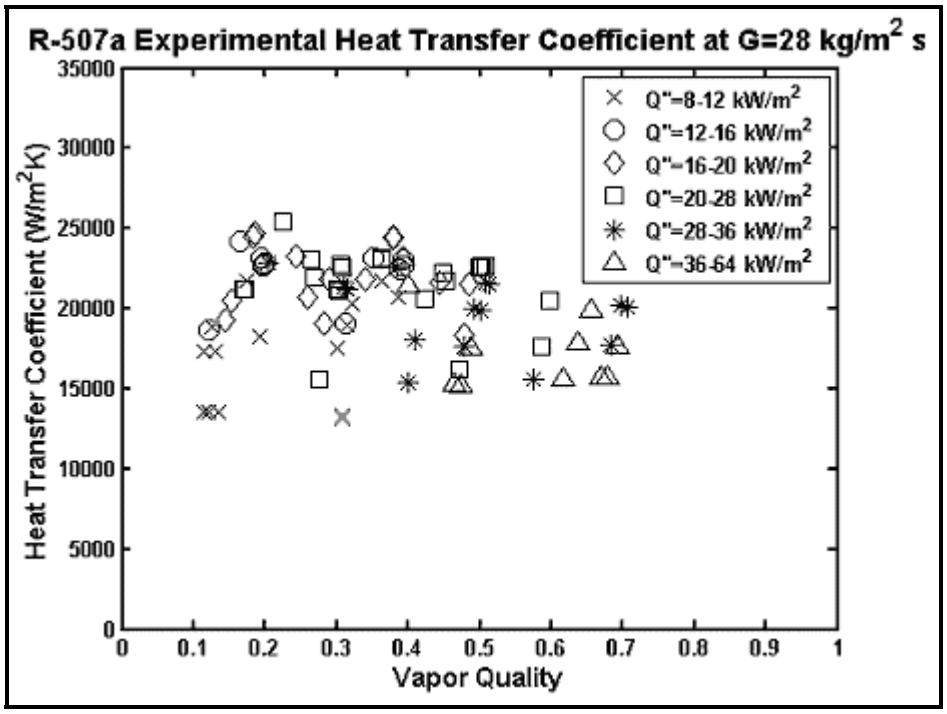

Figure 9.29. Boiling of R-507A on Turbo-Bii tube bundle by Robinson and Thome (2004b).

Most recently, Robinson and Thome (2004b) using the tube bundle layout and experimental technique described above measured local flow boiling heat transfer coefficients for the Turbo-Bii_HP tube for R-134a, R-410A and R-507a, shown respectively in Figure 9.27, Figure 9.28 and Figure 9.29 (note that heat transfer coefficients range from about 15000 to 35000 W/m^{2}K). In these tests they found that convective effects increased local boiling coefficients in the bundle from 10 to 40%, particularly for the low to medium heat fluxes they tested. For comparison, the pool boiling heat transfer coefficient for the Turbo-Bii at q = 16 kW/m^2 for R-134a is 20600 W/m^{2}K, for R-410A is 23650 W/m^{2}K and for R-507A is 21920 W/m^{2}K. The tube was not optimized for use with the last two fluids. The heat transfer coefficients are quite large and yield local boiling superheats on the tubes that are only 0.5-1.0°C (0.9-1.8°F), which results for some of the scatter apparent in their data at these challenging test conditions typical of real operating conditions.

Prediction methods for local bundle boiling heat transfer coefficients are much less advanced than for boiling inside of tubes. Most of the bundle boiling methods available were developed from limited databases, typically obtained only in one laboratory for one or two fluids and hence they cannot be considered to be general methods, likely being unreliable when applied to other fluids, pressures and bundle geometries. Bundle boiling methods have been reviewed in Browne and Bansal (1999), Casciaro and Thome (2001a) and Collier and Thome (1994) while Thome (1990) reviewed enhanced bundle boiling in Chapters 10 to 12. Very few correlations specifically for the prediction of local bundle boiling heat transfer coefficients currently exist. Most of these methods use a modified form of the popular Chen (1963) intube boiling correlation, which thus ignores physical differences between internal and external two-phase flows. Any discussion of the local distribution and interaction of the liquid and vapor phases within a tube bundle must begin with the local void fraction. A new preliminary approach based on local void fraction is presented below (based on limited data like other previous methods).

Thome and Robinson (2006) have proposed a set of empirical bundle boiling heat transfer prediction methods for plain tubes, low finned tubes and enhanced boiling tubes. Their methods are based on only one tube diameter/tube pitch combination (19/22.23 mm, 0.74/0.875 in.), all for tests at one saturation temperature of 5°C (41°F) for an equilateral triangular tube layout. The methods presented below, however, have a general format that allows one to utilize the method for other tube layouts and tube pitches. Also, one can use them for other fluids and tube combinations by inputting one's own nucleate boiling curve. Even so, one must remember that these methods cannot be considered as general correlations because the underlying range of experiments (some described above) was quite limited. The void fraction method of Feenstra, Weaver and Judd (2000) described elsewhere in *Databook III* is used for determining ε in the methods below.

Plain Tube Bundle Boiling Prediction Method. The plain tubes were drawn copper tubes with an untreated surface and were 18.87 mm (0.742 in.) in outside diameter. An asymptotic method was assumed for predicting the local bundle boiling heat transfer coefficient α_{bundle} from the nucleate boiling heat transfer coefficient α_{nb} and the convective boiling heat transfer coefficient α_{cb}:

$$\alpha_{bundle} = \left(\alpha_{nb}^2 + \alpha_{cb}^2\right)^{1/2} \qquad [9.6.1]$$

The nucleate boiling heat transfer coefficient was predicted using the Cooper (1984) dimensional correlation given by [9.3.10], including its 1.7 multiplier that he recommended be applied to copper tubes with a surface roughness set to R_p = 5.7 microns. Utilizing the Cooper correlation to thus calculate α_{nb}, i.e. from its fit to their pool boiling data for R-134a, taking their R-134a experimental local bundle boiling heat transfer coefficients for the values of α_{bundle}, the values of α_{cb} were backed out of the experimental database applying [9.6.1]. The convective heat transfer coefficients thus obtained were assumed to be for heat transfer through a thin liquid film flowing over the tubes in the bundle, i.e. their version of the

sliding bubble heat transfer mechanism proposed by Cornwell (1989), the latter whose photographs can be seen in Figure 9.27 in Collier and Thome (1994). These convective heat transfer values were empirically fit to the following liquid film convection expression:

$$\alpha_{cb} = 4.032\,\mathrm{Re}_{\delta}^{0.236}\,\mathrm{Pr}_{L}^{0.4}\left(\frac{k_L}{\delta}\right) \qquad [9.6.2]$$

In this expression, Pr_L is the liquid Prandtl number, k_L is the liquid thermal conductivity, δ is the liquid film thickness and Re_δ is the liquid film Reynolds number, which is defined as:

$$\mathrm{Re}_{\delta} = \frac{4\rho_L u_L \delta}{\mu_L} \qquad [9.6.3]$$

The mean liquid velocity in the film u_L is:

$$u_L = \frac{\dot{m}_{total}(1-x)}{\rho_L(1-\varepsilon)} \qquad [9.6.4]$$

The mass velocity of the flow is calculated using the minimum cross-sectional area of the bundle (like in single-phase cross flows). The liquid film thickness δ is determined by fitting a hexagonal grid to the tube layout with one tube at the center of each hexagon (see Figure 9.30). Applying the void fraction to this geometry and its cross-sectional flow area, i.e. the area of the hexagon minus that of the cross-sectional area of the tube, the fraction of the area occupied by the liquid-phase is calculated and this area is applied to the perimeter of the tube to find the mean liquid film thickness. Referring to Figure 9.31, the area encompassed by the hexagon, A_{hex} is given by:

$$A_{hex} = 6\left(\frac{L_{pp}}{3}\right)\left(\frac{L_{pn}}{2}\right) \qquad [9.6.5]$$

L_{pp} is the vertical tube pitch and L_{pn} is the horizontal tube pitch. The circumferential flow area A_{cfl} to which the void fraction is applicable is:

$$A_{cfl} = A_{hex} - \frac{\pi D}{4} \qquad [9.6.6]$$

D is the tube outside diameter and the area occupied by saturated liquid A_L in the hexagon is:

$$A_L = A_{cfl}(1-\varepsilon) \qquad [9.6.7]$$

The diameter of the idealized liquid ring created by the liquid film around the tube D_δ is:

$$D_{\delta} = \sqrt{\frac{4A_L}{\pi} + D^2} \qquad [9.6.8]$$

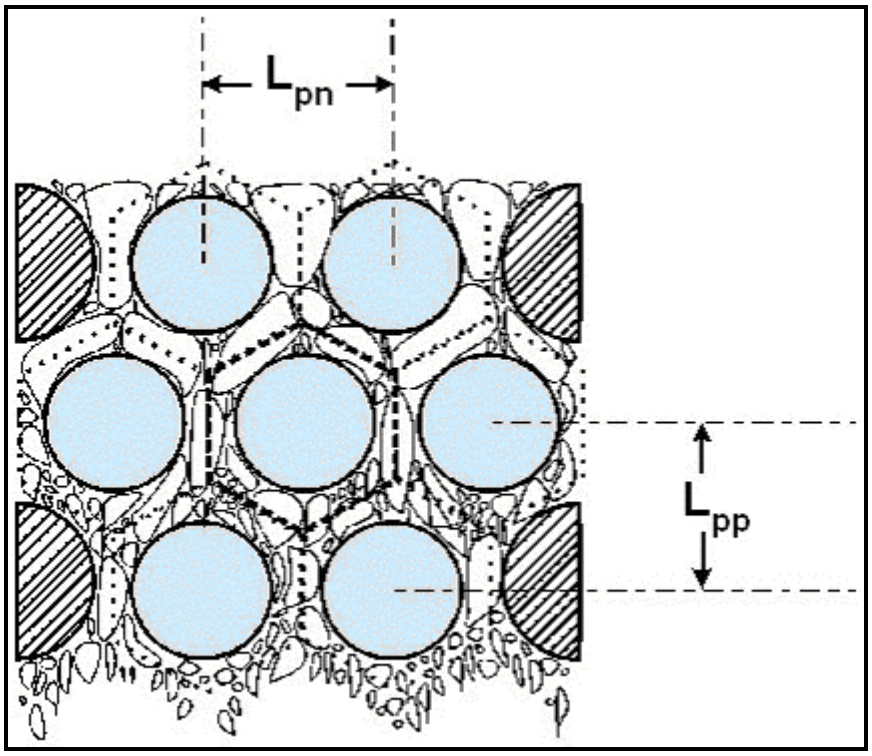

Figure 9.30. Idealized hexagonal grid boundary imposed over bundle cross section to identify local void fraction per tube.

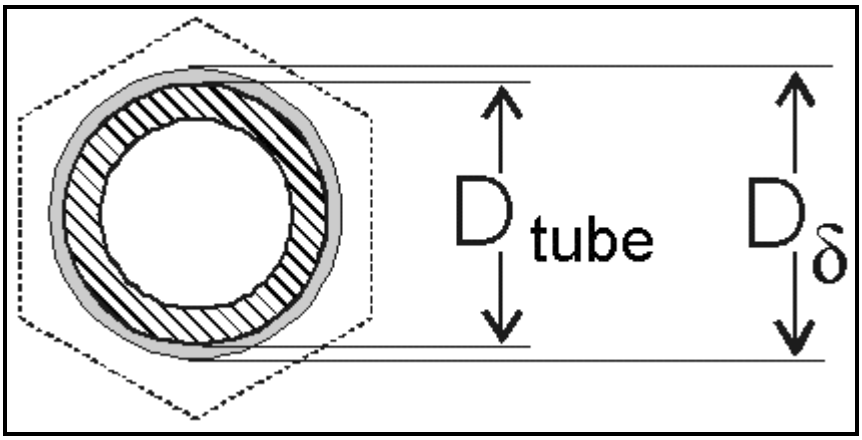

Figure 9.31. Idealized local saturated liquid film surrounding circumference of tube.

The liquid film thickness δ is thus:

$$\delta = \frac{D_\delta - D}{2} \qquad [9.6.9]$$

Though only one tube pitch arrangement was used in the experimental study, the above format is general, allowing future application to other staggered tube layouts, tube diameters and tube pitches similar to the present one.

Figure 9.32 depicts a comparison of the new bundle boiling method to the plain tube bundle boiling database of Robinson and Thome (2004a), capturing a large fraction of the bundle boiling data to within ±20% as shown. The database covers only boiling of R-134a at a saturation temperature of 4.4°C (39.9°F) over the following test conditions: total mass flux from 5 to 41 kg/m^{2}s (3700 to 30300 lb/h ft^2), heat flux from 2 to 35 kW/m^2 (630 to 11100 Btu/h ft^2) and vapor qualities from 10 to 87%. The individual values of the predicted smooth tube nucleate and convective boiling contributions varied greatly with different combinations of heat flux and mass flux. On average, the convective boiling contribution was 63% that of the nucleate boiling contribution, which means that the bundle boiling performance was about 63% higher than that of nucleate pool boiling on a single tube.

Low Finned Tube Bundle Boiling Prediction Method. The Wolverine Turbo-Chil low fin tube bundle (photo of this tube is shown in Figure 9.2) tested in Robinson and Thome (2004c) had a fin density of 1024 fins/meter (26 fins/inch), a root diameter of 15.88 mm, an inside diameter of 14.45 mm (0.569 in.), a fin height of 1.52 mm (0.060 in.) and a fin thickness of 0.2 mm (0.008 in.). These tubes also had an internal enhancement and were tested with a triangular tube pitch of 22.22 mm (0.875 in.). The above asymptotic method was again assumed for predicting the local bundle boiling heat transfer coefficient α_{bundle} for the low finned tube bundle using [9.6.1]. As no reliable method is available for predicting nucleate boiling heat transfer coefficients on low finned tubes, the particular tube's experimentally measured nucleate pool boiling curve was used to determine α_{nb}. For R-507A on the present low finned tube, the experimental boiling curve from their study was:

$$\alpha_{nb} = 93.35 q^{0.448} \qquad [9.6.10]$$

For R-134a on the same low finned tube, the boiling curve was:

$$\alpha_{nb} = 90.11 q^{0.436} \qquad [9.6.11]$$

Note that the heat flux is input in W/m^2 based on the *nominal* surface area of a plain tube with an outside diameter equal to the fin tip diameter and the heat transfer coefficient is given in W/m^{2}K based on this same nominal area (not the total area of the low fin tube). The values of α_{cb} were again backed out from the measured local bundle boiling heat transfer coefficients for α_{bundle} by applying [9.6.1] with the above boiling curves for α_{nb}. The convective heat transfer coefficients were assumed to be a function of liquid flow between adjacent fins but not between adjacent tubes, flows which all turned out to be in the laminar regime. They were empirically fit to a Sieder and Tate (1936) type of laminar convection expression where the exponent on the Reynolds number was found from the data to be only 0.0013. Hence, the expression was reduced to that of a fully-developed laminar flow expression, typical of high aspect ratio rectangular channels, as:

$$\frac{\alpha_{cb} d_h}{k_L} = 13.92 \qquad [9.6.12]$$

In this expression, d_h is the hydraulic diameter for the flow between adjacent fins and is defined as:

$$d_h = \frac{4A_{fa}}{P_L} \qquad [9.6.13]$$

For the flow between two adjacent fins, P_L is the wetted perimeter of the two sides of the fin plus that of the root, so that $P_L = (s - t_{root}) + 2e$ where s in the fin pitch, t_{root} is the fin thickness at its root and e is the fin height. The cross-sectional area A_{fa} for free flow area between two fins is $A_{fa} = (s - t_{root})e$. The use of this laminar channel flow method between the fins was suggested by the void fraction method used for the plain tube bundle described above since the values of the liquid film thickness calculated for the entire wetted surface area of the low-finned tube were typically larger than half the interfin spacing ($s - t_{root}$) and hence the flow between the fins is not a film flow but rather a channel flow.

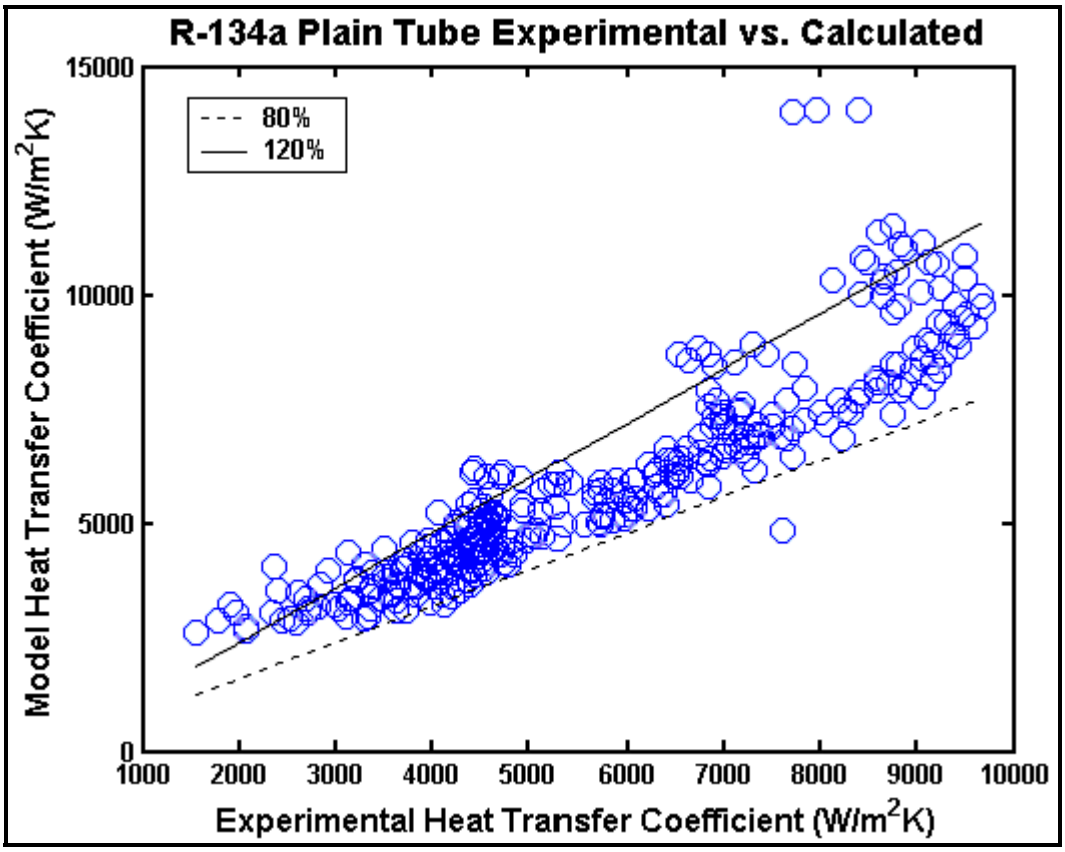

Figure 9.32. Predicted vs. experimental bundle boiling heat transfer coefficients for plain tube.

Figure 9.33 shows the comparison of the above prediction method to the finned tube bundle boiling database for R-134a. Similar results were obtained with R-507A on the same bundle. Most of the data were predicted within ±20%. The database covers only boiling of R-134a and R-507A at a saturation temperature of 4.4 °C (39.9°F) over the following conditions: total mass flux from 3 to 29 kg/m^{2}s (2210 to 21400 lb/h ft^2), heat flux from 2 to 50 kW/m^2 (630 to 15850 Btu/h ft^2) and vapor qualities from 8 to 82%. The individual values of the finned tube nucleate and convective boiling contributions varied greatly with different heat and mass flux conditions; on average the convective boiling contribution was 68% that of the nucleate boiling contribution.

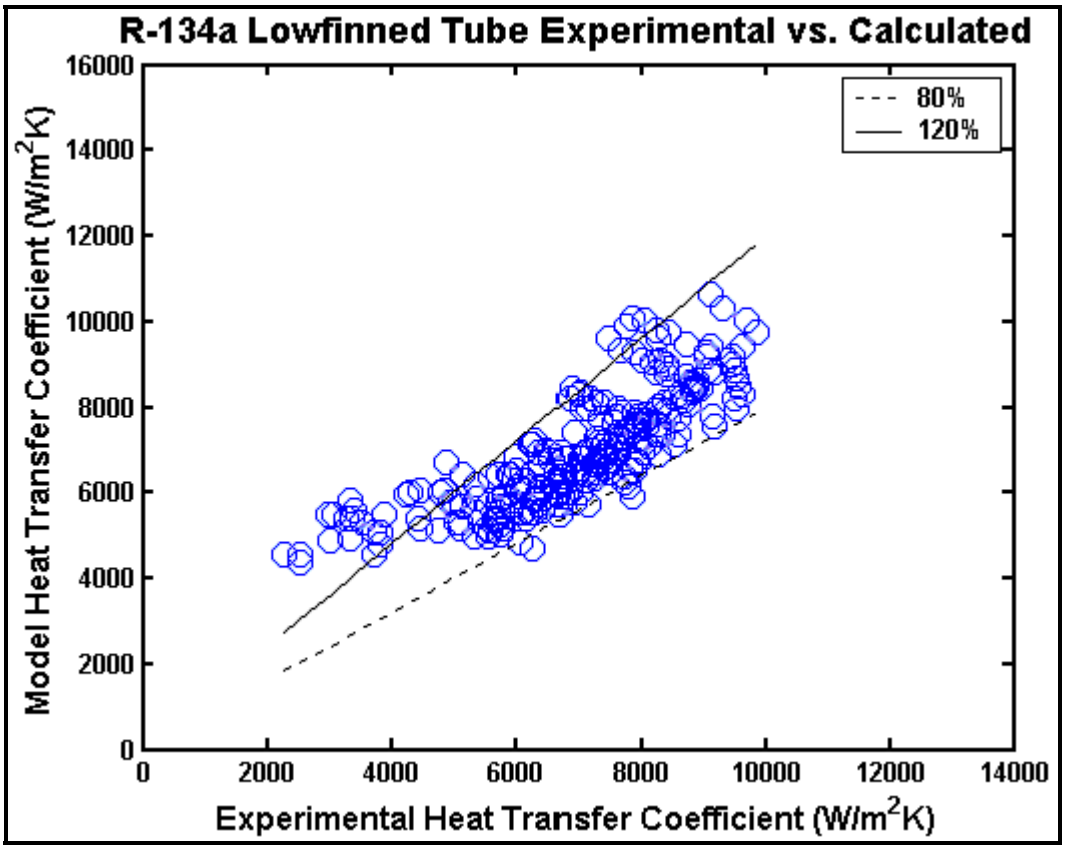

Figure 9.33. Predicted vs. experimental bundle boiling heat transfer coefficients for Turbo-Chil low fin tube.

Turbo-Bii_HP Bundle Boiling Prediction Method. The database of Robinson and Thome (2004b) for tests with R-134a, R-507A and R-410A were used to develop this method. The Wolverine Turbo-Bii_HP tube (shown in Figure 9.4) had a root diameter of 17.48 mm (0.688 in), an outside diameter of 18.69 mm (0.736 in) and an inside diameter of 16.05 mm (0.632 in). They had an internal enhancement and were tested in a bundle with a triangular tube pitch of 22.22 mm (0.875 in.). For predicting the thermal performance of this enhanced boiling tube, another strategy was taken since the convection coefficients α_{cb} deduced for the plain and low finned tube bundles are insignificant with respect to the Turbo-Bii_HP bundle performance because of its very high nucleate boiling coefficients, i.e. such α_{cb} values are on the order of 1 kW/m^{2}K whereas those of α_{nb} are on the order of 20 to 25 kW/m^{2}K). The bundle boiling effect (local bundle heat transfer coefficient relative to their corresponding value of α_{nb}) was significant as described in Robinson and Thome (2004b). Furthermore, it did not seem justified to multiply α_{cb} in [9.6.2] by factors up to 5 to account for the "rough" surface of the Turbo-Bii_HP tube. They thus concluded that the two-phase flow had an enhancing effect on the nucleate boiling process itself, perhaps by increasing the departure frequencies of the bubbles leaving the re-entrant channels, which in turn would augment the thin film evaporation and convection processes inside the re-entrant channels. Hence, a bundle boiling factor approach was taken to predict the local bundle boiling heat transfer coefficients α_{bundle} for the Turbo-Bii_HP tube bundle as:

$$\alpha_{bundle} = \alpha_{nb} F_p F_\varepsilon \qquad [9.6.14]$$

In the absence of a pool boiling correlation to predict α_{nb} for this tube, the experimental nucleate boiling curves for the particular fluid boiling on Turbo-Bii_HP were used to calculate α_{nb}. The nucleate pool boiling curves from Robinson and Thome (2004b) for the three fluids were:

R-134a: $$\alpha_{nb} = 30944 q^{-0.042} \quad [9.6.15]$$

R-507A: $$\alpha_{nb} = 37334 q^{-0.055} \quad [9.6.16]$$

R-410A: $$\alpha_{nb} = 43520 q^{-0.063} \quad [9.6.17]$$

Here, α_{nb} was nearly insensitive to heat flux. Their bundle boiling reduced pressure correction factor F_p, in terms of the reduced pressure p_r, was:

$$F_p = 1.41 - 2.66 p_r \quad [9.6.18]$$

Their bundle boiling void fraction correction factor F_ε was correlated as:

$$F_\varepsilon = 1.15 - 2(0.4 - \varepsilon)^2 \quad [9.6.19]$$

In this last expression, the local void fraction is calculated with the tube bundle void fraction method of Feenstra, Weaver and Judd (2000). The void fractions in the tests ranged from 0.16 to 0.85 while the reduced pressures ranged from 0.084 to 0.2. A maximum in the bundle effect for all three fluids occurred at a void fraction of about 0.4, above which the heat transfer performance fell off. The bundle effect was observed experimentally to decrease with increasing reduced pressure and hence the introduction of the factor F_p. Due to the highly empirical nature of this method and the limited database, it is recommended that caution be used in extrapolating this method outside of its present range of reduced pressures and void fractions.

Figure 9.34 shows their R-134a bundle boiling data compared to the prediction method, with the data segregated by measurement location, dividing them into one set that is for the bottom tube row in the bundle and the other set for upper tube rows (tube rows 3, 5 and 7 counting from the bottom up). As can be seen, the bottom tube row data tend to differ from the other tube rows. Two explanations were offered for this. First of all, the hot water inside the tubes in the bundle entered at the top and hence the water temperature profile became rather flat in the bottom tube row, so those experimental values were more sensitive to the measured slope of the water temperature profile than the others. The bottom row data in fact were grouped by location along the tube, where the left-most data are for the last test location along the bottom tube before the hot water exits the bundle and the right-most are for the first test location along the bottom tube. Secondly, there could have been an "entrance effect" on the bottom tube row since no bubble jet from lower boiling tubes impinges on it. The first case seemed to be the most plausible explanation. Hence, disregarding the data from the last two locations on the bottom tube row, the comparison of the prediction method to the remaining database was quite satisfactory, also for R-410A and R-507A where the same trends were observed, and most of such data were predicted within ±20%. The database covered R-134a, R-507A, and R-410A at a saturation temperature of 4.4 °C (39.9°F) for: total mass flux from 4 to 38 kg/m^{2}s (2950 to 28040 lb/h ft^2), heat flux from 8 to 64 kW/m^2 (2540 to 20290 Btu/h ft^2) and vapor qualities from 8 - 78%.

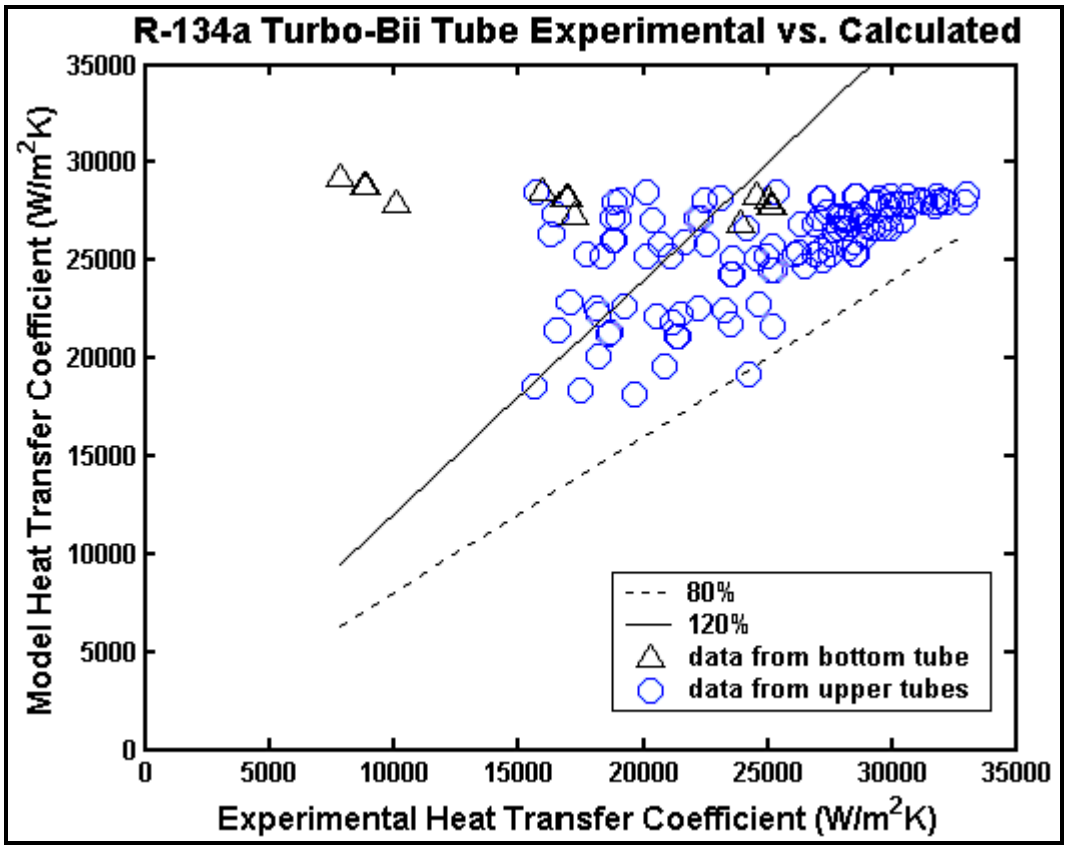

Figure 9.34. Predicted vs. experimental bundle boiling heat transfer coefficients for Turbo-Bii_HP tube.

9.7 Dryout Mechanisms on Bundle Boiling

The upper operating limit of plain and enhanced tube bundles is governed by several possible dryout scenarios. These have been contemplated for those occurring on horizontal kettle reboilers widely used in petro-chemical applications and are in part also applicable to flooded evaporators favored by the refrigeration industry. Figure 9.35 illustrates these. Mechanism (a) is for small tube bundles with few tube rows; here, the maximum heat flux is essentially limited by that for DNB on a single tube, i.e. by expression [9.3.18]. Mechanism (b) refers to a unit with liquid loading onto the bundle from above, where the liquid loaded from above is not able to penetrate to the bottom of a large bundle because of the up flow of the vapor. Mechanism (c) occurs for large tube bundles with too little inflow from beneath, which can create unfavorable circulation of liquid and mal-distribution of liquid in the bundle and hence local dryout. Mechanism (d) refers to another circulation-limited problem in which the bundle is starved for liquid and locally dries out. Mechanism (e) describes the onset of mist flow that can occur at high local vapor qualities where all the liquid is entrained as tiny droplets into the vapor flow.

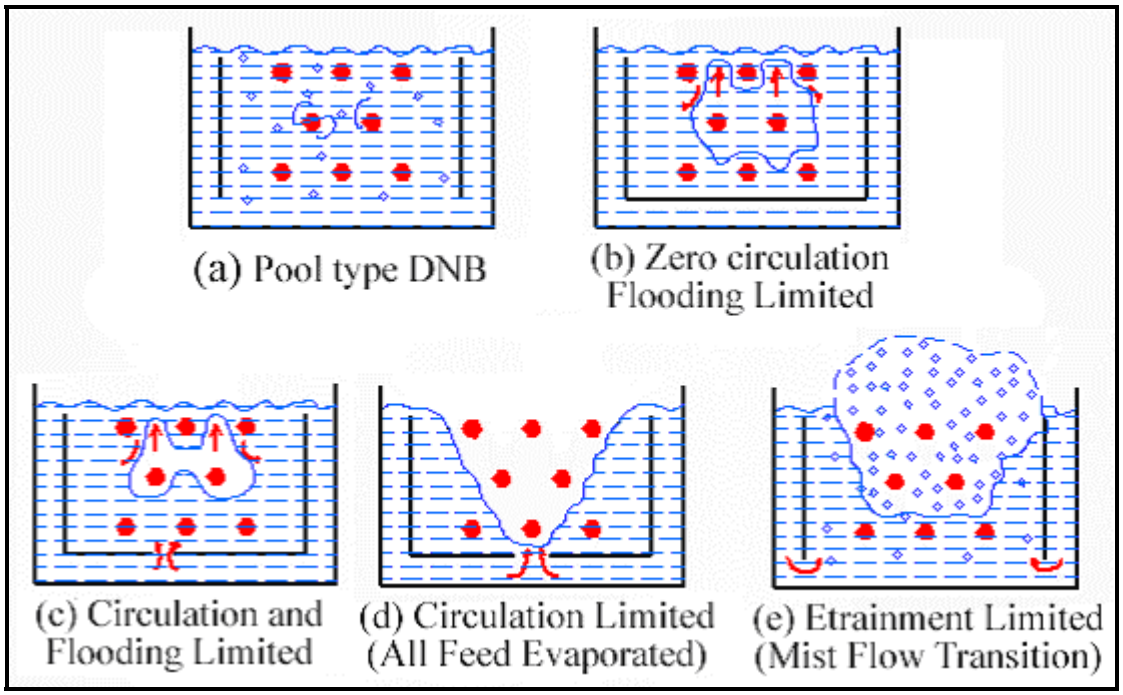

Figure 9.35. Dryout mechanisms on horizontal tube bundles.